PHYSICAL REVIEW B VOLUME 2, NUMBER 9 1 NOVEMBER 1970

Spectroscopy of Kondo and Spin-Flip Scattering: High-Field Tunneling Studies of Schottky-Barrier Junctions

E. L. Wolf* and D. L. Losee*
Research Laboratories, Eastman Kodak Company, Rochester, New York 14650
(Received 4 May 1970)

A comprehensive study of the energy, temperature, and magnetic field dependence of the anomalous Kondo and spin-flip conductances $G^{(3)}(V)$ and $G^{(2)}(V)$, in vacuum-cleaved metal-semiconductor tunnel junctions is reported. Localized Anderson magnetic moments are characteristic of Schottky barriers at donor concentrations a few times the Mott critical concentration N_c. These moments, coupled to the conduction electrons in the semiconductor by the s-d exchange interaction $-2J\vec{S}\cdot\vec{\sigma}$, are lightly screened neutral donors at the inner edge of the depletion region. The background conductance in vacuum-cleaved junctions on Si: (1.6×10^{19} cm^{-3} donors) agrees satisfactorily with the parabolic barrier model, extended to the thin-barrier limit. A detailed study shows the energy dependence of the zero-bias Kondo scattering peak $G^{(3)}(V)$ to be in good agreement with the third-order perturbation theory of Kondo and Appelbaum. High magnetic field studies confirm that a large negative g shift $\Delta g = 2J\rho_F \sim -1.0$ and related broadening $\Gamma = \pi(J\rho_F)^2 g\mu_B H$ of the Zeeman transition of the local moment occur via the exchange interaction. The broadening Γ additionally produces, for $\Gamma \gg k_B T$, a quenching of the Kondo scattering peak from $-\log T$ to $-\log(\Gamma/k_B)$. The directly measured parameters $J\rho_F$ and E_0 determine a divergence temperature $T_K = (E_0/k_B) \times \exp(1/J\rho_F) = (2\pm1)$ °K, significantly higher than an upper bound ~ 0.5 °K, indicated by the observed accurate $\log T$ dependence of $G^{(3)}(0)$ to 0.4 °K. The discrepancy is removed by assuming simultaneous potential and exchange scattering in a ratio determined via Appelbaum's theory from the observed ratio $G^{(3)}/G^{(2)}$. In summary, the tunneling spectra and an extended Kondo-Appelbaum perturbation theory, including the implied g shift, broadening Γ, and an added potential scattering, are in good agreement.

I. INTRODUCTION

Interest has developed in the problem of exchange scattering of electrons from dilute paramagnetic impurities in metals since Kondo showed that an exchange coupling,

$$H^x = -2J\vec{S}\cdot\vec{\sigma}\,, \tag{1.1}$$

leads to a divergent third-order scattering with a $-\log T$ temperature dependence, which explains the low-temperature resistivity minimum common in dilute alloys.[1] Here $\vec{S}$ and $\vec{\sigma}$ represent the spin of the localized magnetic moment and a conduction electron, respectively, and J is the exchange-coupling energy. This interest has been enhanced more recently by theoretical arguments [2-5] that in the limit of strong coupling or low temperatures, when the perturbation series can no longer be assumed to converge, a new physical state might appear. The new regime, which is expected to appear below a temperature T_K, is characterized by standing waves of electrons of opposite spin projection in the vicinity of each local impurity moment. This state has been described as quasibound[4] and as a scattering resonance.[3,5] The characteristic temperature T_K is given by a relation of the form

$$T_K = (E_0/k_B)e^{1/J\rho_F}, \tag{1.2}$$

where J is the exchange energy, E_0 an energy cutoff, and ρ_F the density of states. T_K does not sharply define a transition, but rather sets a temperature scale on which departures from perturbation-theory estimates of, e.g., susceptibility and resistivity should appear.

This paper is not primarily concerned with the proposed quasibound state. Indeed, our experiments show no evidence for a separate low-temperature behavior. We expect, however, that the techniques which we have employed will be extended to lower temperatures and/or to junctions with stronger coupling in which these effects should be important, and will provide a definitive test of the several theories.

We shall describe tunneling experiments that provide a direct spectroscopy of the spin-flip and Kondo scattering associated with the exchange interaction (1.1). In zero external magnetic field, the experiment measures directly the energy dependence of the third-order scattering rate $W_{ij}^{(3)}$, whereas in high fields we will see that the exchange-coupling parameter $J\rho_F$ can be inferred from the energy dependence of the inelastic spin-flip scattering $W_{ij}^{(2)}$.

Magnetic moments localized near one edge of a suitable tunnel junction may have an exchange coupling $J\rho_F$ to conduction electrons in the electrode comparable in magnitude to couplings present in dilute magnetic alloys. Figure 1 shows schematically

the location of the moments near the right-hand (a) side of a barrier. Detailed theoretical work by Appelbaum[6] and by Anderson,[7] employing the tunneling Hamiltonian formalism, has shown that Kondo scattering attenuated by a barrier transmission factor $T_J^2 \sim e^{-2\kappa t}$ can transfer electrons across the barrier, thus contributing to a measurable current j.

To understand this exchange-tunneling version of Kondo scattering, we first write the transition probability per unit time W_{ij} for an interaction Hamiltonian H', including the third-order term

$$W_{ij} = \frac{2\pi}{\hbar}\left(|H'_{ij}|^2 + \sum_{k\neq i} \frac{H'_{ik}H'_{kj}H'_{ij}}{E_i - E_k} + \text{c.c.}\right) . \quad (1.3)$$

If we let $H' = H^x$ from (1.1) and restrict the conduction electron $\vec{\sigma}$ to the right-hand electrode, W_{ij} will give the spin-flip ($|H^x_{ij}|^2$) and Kondo (third-order) scattering rates between the states i and j in the a electrode: No tunneling is involved. The operator H^x may also be written as

$$H^x = -J\sum_{k,k'} [S_z(a^\dagger_{k+}a_{k'+} - a^\dagger_{k-}a_{k'-}) + S^+(a^\dagger_{k-}a_{k'+}) + S^-(a^\dagger_{k+}a_{k'-})] , \quad (1.4)$$

where a_k and $a_k^\dagger$ are annihilation and creation operators for an electron of wave vector k in the (a) electrode and the $S^\pm$ operators are raising and lowering operators for the z projection of the localized spin operator $\vec{S}$. If we simply replace $a^\dagger$ by $b^\dagger$ in this expression, we have one part of the exchange-tunneling operator H^{Tx}; if we replace a by b, we have the other part:

$$H^{Tx} = -T_J\sum_{k,k'} [S_Z(b^\dagger_{k+}a_{k'+} - b^\dagger_{k-}a_{k'-}) + S^+(b^\dagger_{k-}a_{k'+}) + S^-(b^\dagger_{k+}a_{k'-}) + S_Z(a^\dagger_{k+}b_{k'+} - a^\dagger_{k-}b_{k'-}) + S^+(a^\dagger_{k-}b_{k'+}) + S^-(a^\dagger_{k+}b_{k'-})] . \quad (1.5)$$

This operator leads to electron transfers across the barrier in which the tunneling electron and local moment may reverse their spin projections. [If we regard the a and b electrodes as part of a total system, H^x and H^{Tx} are two contributions to a total exchange interaction (1.1).] Since H^{Tx} involves electrons on opposite sides of the barrier, its matrix element T_J will be smaller than J by a factor of approximately $e^{-\kappa t}$, where κ is the decay constant and t the thickness of the barrier.

The rate W_{ij} for a tunneling transition, where i and j now contain conduction-electron states on opposite sides, can be obtained by setting

$$H' = H^x + H^{Tx} + H^T . \quad (1.6)$$

H^T includes the usual elastic tunneling. Upon substituting Eq. (1.6) into Eq. (1.3), Appelbaum[6] finds in the tunneling rate W_{ij} terms

$$W^{(2)}_{ij} = (2\pi/\hbar)|H^{Tx}_{ij}|^2 \sim T_J^2 \quad (1.7)$$

and

$$W^{(3)}_{ij} = \frac{2\pi}{\hbar}\left(\sum_{i\neq k} \frac{H^{Tx}_{ik}H^{Tx}_{kj}H^x_{ij}}{E_i - E_k} + \text{c.c.}\right) \sim T_J^2 J , \quad (1.8)$$

in addition to other nonexchange terms (e.g., elastic tunneling $T^2 \sim e^{-2\kappa t}$). These two terms correspond, respectively, to spin-flip and "anomalous" third-order (Kondo) scattering across the barrier, since H^{Tx}[Eq. (1.5)] and H^x [Eq. (1.4)] involve the same spin operators $\vec{S}$. These transition probabilities, in fact, differ from the usual spin-flip and Kondo scattering rates only by a scale factor $\sim e^{-2\kappa t}$. As we shall see, the characteristic energy (i.e., bias voltage), temperature, and magnetic field dependences of $W^{(2)}_{ij}$ and $W^{(3)}_{ij}$ permit their separation from other contributions to the total transition rate across the barrier.

Kondo[1] showed that the anomalous $-\log T$ behavior originates in $W^{(3)}_{ij}$, Eq. (1.8), from those intermediate states k reached by a spin flip of the local moment. The E_k in the denominator of (1.8) are intermediate-state energies of the conduction-electron–localized-moment combination. Thus $E_i - E_k = \epsilon_i - \epsilon_k - \Delta$, where the ϵ's are conduction-electron energies and Δ is any energy associated with the spin-flip transition of the moment. Kondo explicitly requires that an unoccupied intermediate state ϵ_k is available for the conduction electron performing

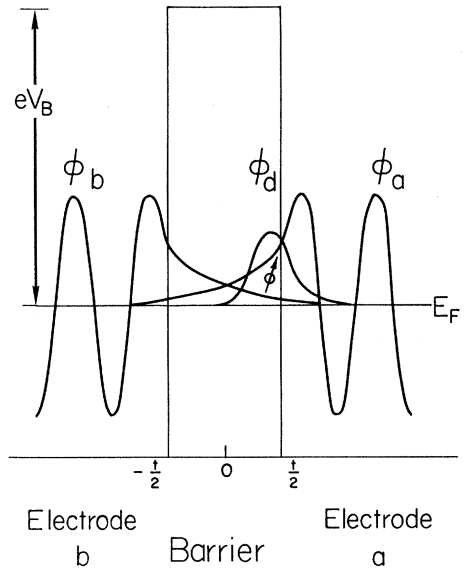

FIG. 1. Schematic diagram of tunnel junction. Localized magnetic state ϕ_d strongly overlaps conduction-electron wave functions in the a electrode. Weaker interaction with b electron wave functions leads to exchange-tunneling events.

the initial transition $\epsilon_i \to \epsilon_k$ by weighting the corresponding terms in the sum by $1-f(\epsilon_k)$, where f is the Fermi function. If the conduction-electron intermediate state is initially occupied, on the other hand, the scattering can proceed as $\epsilon_k \to \epsilon_j$ followed by $\epsilon_i \to \epsilon_k$; in this alternative process, weighted by $f(\epsilon_k)$, a portion of the spin-matrix element occurs with a *negative sign*. Thus the Fermi functions do not disappear, as in potential scattering, but add as $1-2f(\epsilon_k) \equiv \tanh(\frac{1}{2}\beta\epsilon_k)$, where $\beta = (k_B T)^{-1}$. In a standard approximation, the third-order contribution becomes

$$W_{ij} \propto \delta(E_i - E_j)\, T_J^2\, J\rho(E_F)\, P \int_{-E_0}^{E_0} \frac{\tanh(\frac{1}{2}\beta\epsilon)\, d\epsilon}{E_i - \epsilon} . \tag{1.9}$$

This integral contains the logarithmic energy and temperature dependence characteristic of Kondo scattering. An important assumption in this formulation is that the intermediate states k have energies $E_k = \epsilon_k + \Delta$ sharp compared to $k_B T$.

The energy dependence of the scattering is directly revealed in the voltage derivative of the tunneling current $j(V)$. In particular, the contribution to the conductance $G(V) \equiv (\partial/\partial V) j$ of the third-order scattering $W_{ij}^{(3)}$, Eq. (1.9), is given by Appelbaum[6] as

$$G^{(3)}(V) = \alpha\, T_J^2 (J\rho_F) \int_{-\infty}^{\infty} \int_{-E_0}^{E_0} \frac{\tanh(\frac{1}{2}\beta\epsilon)}{E - \epsilon} \times \frac{d}{dE} f(E - eV)\, d\epsilon\, dE \quad \text{for } H = 0. \tag{1.10}$$

Since at low temperature $(\partial/\partial E) f(E - eV)$ is sharply peaked at $eV = E$, with width $\sim 2k_B T$, $G^{(3)}(V)$ is an accurate measure of $W_{ij}^{(3)}(eV)$. Similarly, the second-order transition probability $W_{ij}^{(2)}$ produces an analogous conductance $G^{(2)}(V, H)$. This contribution, corresponding to spin-flip scattering, becomes inelastic in a magnetic field H, as the tunneling electron must supply the excitation energy $g\mu_B H = \Delta$. A characteristic increase in $G^{(2)}(V, H)$ occurs at $V = \pm \Delta/e$, and the Zeeman transition line shape of the local moment may be displayed directly by measuring the derivative $(d/dV) G^{(2)}(V, H)$. This peak represents the Zeeman transition for the local moment *as it is coupled* to the conduction electrons in the nearby electrode. Thus, an appropriate spin Hamiltonian should contain the assumed exchange coupling (1.1):

$$H_s = -g_0 \mu_B \vec{S} \cdot \vec{H} - 2J \textstyle\sum_i \vec{S} \cdot \vec{\sigma}_i . \tag{1.11}$$

In an applied field H, the conduction electrons $\vec{\sigma}_i$ are polarized by the field; hence the summation is proportional to $P = \chi H$. Both terms in the spin Hamiltonian are thus proportional to H and an effective g value is obtained [8-10] by collecting the coefficients of H:

$$g = g_0 + 2J\rho_F . \tag{1.12}$$

This "Knight shift" $2J\rho_F$ is obtained taking for χ the Pauli-spin susceptibility. If the value g_0 is known, the coupling parameter $J\rho_F$ can be obtained[11] from the g value of the $(d/dV) G^{(2)}(V, H)$ "resonance." The coupling H^x also produces rapid spin-flip exchanges between the local moment and conduction electrons in the nearby electrode.

The corresponding lifetime broadening[9,10] of the Zeeman transition is related to the g shift by a Korringa-like formula

$$\Gamma = \hbar/T_1 = \pi (J\rho_F)^2 \Delta \tag{1.13}$$

for $\Delta = g\mu_B H \gg k_B T$. The proportionality to H appears because the number of conduction electrons able to accept energy Δ in deexcitation of the local moment is proportional to Δ.

Finally, we note that in high magnetic fields, the presence of the inherent lifetime broadening Γ, Eq. (1.13), must be taken into account in the third-order scattering, as it broadens the intermediate spin-flipped states E_k, and for $\Gamma \gg k_B T$ reduces the Kondo scattering rate from $-\log T$ to $-\log(\Gamma/k_B)$.[12]

The parameter $J\rho_F$ determines the size of these effects. It is basically this parameter which determines the ratio of Kondo scattering to spin-flip scattering. As we shall see, there is no reason to assume $-J\rho_F$ to be small; it may easily be greater than 0.25.

In previously reported [13] studies, zero-bias conductance peaks in metal-insulator-metal tunnel junctions have also been interpreted in terms of Appelbaum's theory.[6] A recent review,[14] however, has concluded that the reported verification of Kondo scattering $G^{(3)}$ should be regarded as tentative, since the magnetic field dependence was interpreted entirely in terms of second-order scattering. On the contrary, we find that the equivalent assumption, that $G^{(3)}$ is independent of magnetic field, is invalid.[12] Other advances represented in the present study are that the tunneling barrier and background conductance spectrum are understood quantitatively, a microscopic model[11] of the local moment is available, the voltage dependence $G^{(3)}(V)$ at zero field is carefully compared with the Kondo integral, and the g shift and associated broadening are recognized as essential to the physics and are studied experimentally,[11,12] allowing us to predict the characteristic temperature T_K.

This paper reports fully an experimental study of spin-flip and Kondo scattering in vacuum-cleaved metal-semiconductor (Schottky-barrier) tunnel junctions.[15-17] This type of junction is unique in the degree to which its chemical composition can be specified. As indicated in Fig. 2, the tunneling barrier lies entirely in the semiconductor (shown as N type) whose properties are well understood.

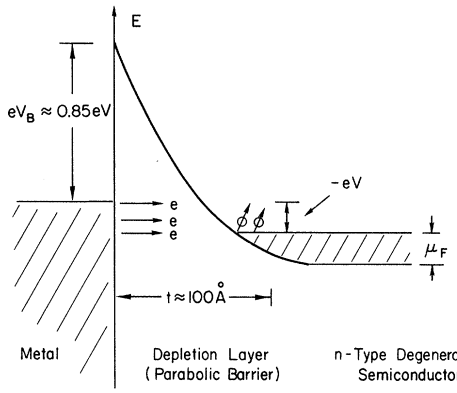

FIG. 2. Schematic diagram of a Schottky-barrier junction on degenerate N-type semiconductor. Values indicated are appropriate to silicon at donor concentration $N_D \approx 10^{19}\,\text{cm}^{-3}$. Conduction-band edge represents the energy of any of the equivalent $\vec{k}_0$ minima. Localized magnetic moments occur at inner edge of depletion region.

Further, the quadratic variation of the band-edge energy with position in the semiconductor depletion region, which follows from Poisson's equation, defines an average tunneling barrier for which the electron penetration and transmission have been calculated exactly.[16] Zero-bias conductance peaks $G^{(3)}(V)$ are a characteristic feature of such Schottky-barrier tunnel junctions for donor (or acceptor) concentrations several times the Mott critical concentration N_c.[11] The magnetic moments inherent in such junctions are lightly screened neutral donor states localized at the inner edge of the depletion region. Such $S=\frac{1}{2}$ moments are relatively simple and are well described by the Anderson model.[7] Some of their properties can be inferred from the well-known magnetic and optical properties of noninteracting shallow donors.

We shall see that two basic physical models, the parabolic barrier[16] and the localized donor model of the magnetic moment, together with an extended Appelbaum-Kondo theory,[6] permit a semiquantitative understanding of all features of both the elastic background conductance and the magnetic scattering conductance.

We now summarize the theoretical considerations necessary to understand the experimental results.

II. THEORETICAL CONSIDERATIONS

A. Exchange Tunneling in Magnetic Field

The purpose of this section is to summarize Appelbaum's tunneling Hamiltonian theory[6] of the exchange-tunneling conductance in the presence of a magnetic field.

In the tunneling Hamiltonian approach,[14] the junction is regarded as two nearly isolated systems described by H^a and H^b, which are weakly coupled by a barrier region, as indicated in Fig. 1. Note that the barrier is included in both systems, and that, e.g., wave function ϕ_a oscillates to the right of $\frac{1}{2}t$ and decays exponentially in the barrier to the left of $\frac{1}{2}t$. A single magnetic state ϕ_d is located at the right-hand (a electrode) side of the barrier. Since the a and b systems are nearly isolated, one can speak of eigenstates ϕ_{ka} and ϕ_{kb} of Hamiltonians H^a and H^b, with energies ϵ_k^a and ϵ_k^b, respectively. It is plausible that an operator H' should describe the coupling between the a and b systems afforded by the potential barrier and the localized magnetic state ϕ_d. One can then use perturbation theory to calculate the corresponding rate W_{ij} for transitions between states i and j which differ by the transfer of one electron across the barrier:

$$W_{ij}=\delta(E_i-E_j)\frac{2\pi}{\hbar}\left(|H'_{ij}|^2+\sum_{k\neq i}\frac{H'_{ik}H'_{kj}H'_{ij}}{E_i-E_k}+\text{c.c.}+\cdots\right). \tag{2.1}$$

The state i, of energy E_i, in general will describe a conduction electron of energy ϵ_i plus the localized electron ϕ_d, which may have its spin projection M changed in a transition $i\to j$. The resulting current density is

$$j(V)=e\sum_m P_M\sum_{ij}W_{ij}f(\epsilon_i^a)[1-f(\epsilon_j^b+eV)] - e\sum_m P_M\sum_{ij}W_{ji}f(\epsilon_j^b+eV)[1-f(\epsilon_i^a)]. \tag{2.2}$$

Here i and j imply quantum numbers $\vec{k}$, $\vec{\sigma}$, and M, representing, respectively, the wave vector and spin of the conduction electron and spin projection of the local moment; $f(\epsilon)$ is the Fermi function; P_M is the probability of a spin projection M; and the applied bias voltage is V. The conductance

$$G(V)\equiv\frac{d}{dV}j \tag{2.3}$$

is the quantity normally measured, as it contains the most direct physical information. Appelbaum expresses the Hamiltonian H of the total system in terms of field operators $\Psi^\dagger(\vec{r})$ and $\Psi(\vec{r})$, such that $\Psi^\dagger(\vec{r})\Psi(\vec{r})$ is the electron density operator at $\vec{r}$:

$$H=\int\Psi^\dagger(\vec{r})[p^2/2m+V(\vec{r})]\Psi(\vec{r})\,d^3r + \tfrac{1}{2}\int\int\Psi^\dagger(\vec{r})\Psi^\dagger(\vec{r}')W(\vec{r}-\vec{r}')\Psi(\vec{r}')\Psi(\vec{r})\,d^3r\,d^3r'\,. \tag{2.4}$$

Here $W(\vec{r}-\vec{r}')$ is the electron-electron interaction and is included to treat exchange interactions with the state ϕ_d. The next step is to expand the creation operator in terms of the states of physical interest:

$$\Psi^\dagger(\vec{r})=\sum_k a_k^\dagger\phi_{ka}(\vec{r})+\sum_{k'}b_{k'}^\dagger\phi_{k'b}(\vec{r})+\sum_M d_M^\dagger\phi_d(\vec{r}-\vec{R})\,. \tag{2.5}$$

Here $d_M^\dagger$ creates an electron of spin projection M in state ϕ_d. Direct substitution of (2.5) [and the anal-

ogous expression for $\Psi(\vec{r})$] into (2.4) generates a number of terms, which are classified by the creation and annihilation operators they contain. Thus

$$\sum_k \epsilon_k^a a_k^\dagger a_k \quad \text{and} \quad \sum_{k'} \epsilon_{k'}^b b_{k'}^\dagger , \tag{2.6}$$

where the ϵ_k's are electron energies on the a and b sides, respectively, belong in H^a and H^b. On the other hand, terms like

$$\sum_{\vec{k},\vec{k}'} T_{kk'} a_k^\dagger b_{k'}, \tag{2.7}$$

which correspond to electron annihilation on one side and creation on the other, belong in H', and describe the usual elastic tunneling.

Tunneling accompanied by interaction with the localized state ϕ_d is described by

$$\sum_{k,k'} W_{k,k'} a_k^\dagger d_M^\dagger b_{k'} d_M, \tag{2.8}$$

which for $M \neq M'$ implies a spin flip of the local moment on ϕ_d.

Interaction of the local state with electrons in the nearby (a) electrode is described by

$$\sum_{k,k'} W_{kk'} d_M^\dagger a_k^\dagger d_{M'} a_{k'} . \tag{2.9}$$

Terms (2.8) and (2.9) contribute to "exchange tunneling" with matrix element T_J and to the exchange interaction J, respectively.

It is useful to express the d operators in terms of spin operators, through the relations

$$S^+ = d_+^\dagger d_-, \quad S^- = d_-^\dagger d_+, \quad S_z = \tfrac{1}{2}(d_+^\dagger d_+ - d_-^\dagger d_-) . \tag{2.10}$$

Finally, the terms in H' are given[6] as

$$H' = H^T + H^{Tx} + H^x, \tag{2.11}$$

$$H^{Tx} = -T_J \sum_{kk'} \{S_z[(a_{k+}^\dagger b_{k'+} - a_{k-}^\dagger b_{k'-}) + \text{c.c.}] + S^+(a_{k-}^\dagger b_{k'+} + b_{k-}^\dagger a_{k'+}) + S^-(a_{k+}^\dagger b_{k+} + b_{k+}^\dagger a_{k-})\}, \tag{2.12}$$

$$H^T = (T + T_A)\sum_{kk'M} (a_{kM}^\dagger b_{k'M} + b_{kM}^\dagger a_{k'M}), \tag{2.13}$$

$$H^x = -J\sum_{k,k'} [S_z(a_{k+}^\dagger a_{k'+} - a_{k-}^\dagger a_{k'-}) + S^-(a_{k+}^\dagger a_{k'-}) + S^+(a_{k-}^\dagger a_{k'+})]. \tag{2.14}$$

The magnetic field $\vec{H}$ and applied bias energy eV appear in H^0:

$$H^0 = \sum_k \epsilon_k^a a_k^\dagger a_k + \sum (\epsilon_k^b + eV) b_k^\dagger b_k - g\mu_B \vec{S}\cdot\vec{H} . \tag{2.15}$$

Equation (2.14) is equivalent to Eq. (1.1) and represents the s-d exchange interaction. In our sign convention, which differs from that of Appelbaum, $J<0$ implies antiferromagnetic coupling. H^{Tx} differs from H^x only by the appearance of electron creation operators from both sides of the junction. The matrix elements J and T_J are formally

$$J = \int\int \phi_j^b(\vec{r}_1)\phi_d(\vec{r}_2) W(\vec{r}_1 - \vec{r}_2)\phi_d(\vec{r}_2)\phi_j^b(\vec{r}_1)\, d\tau_1\, d\tau_2, \tag{2.16}$$

$$T_J = \int\int \phi_i^a(\vec{r}_1)\phi_d(\vec{r}_2) W(\vec{r}_1 - \vec{r}_2)\phi_d(\vec{r}_1)\phi_j^b(\vec{r}_2)\, d\tau_1\, d\tau_2 . \tag{2.17}$$

Roughly T_J is smaller than J by a factor $e^{-\kappa t}$. $W(\vec{r}_1 - \vec{r}_2)$ is not simply $e^2/\epsilon r_{12}$, which gives $J>0$ (ferromagnetic coupling), but is dominated by a mixing effect[18] which gives $J<0$.

The conductance is obtained by inserting the effective Hamiltonian H' of Eqs. (2.11)–(2.15) into expression (2.1) for the transition rate W_{ij}. Of the terms generated, Appelbaum selects as important those of order $(T+T_A)^2$, $(T+T_A)T_J$, and, most importantly, those of order T_J^2 and $T_J^2 J$, which correspond, respectively, to spin-flip tunneling and Kondo tunneling. In these latter cases, the matrix element squared of the raising or lowering operator for the spin S may be a factor in W_{ij}.[1,6] In calculating the current contributions from these magnetic scattering rates from Eq. (2.2), it is necessary to sum over the spin projections M of the localized moment. In thermal equilibrium, the magnetization $\langle M\rangle$ is

$$\langle M\rangle = \sum_{M=-S}^{S} P_M M = B_S\left(\frac{\Delta}{k_B T}\right) \to \tanh\left(\frac{\Delta}{2k_B T}\right), \quad S=\tfrac{1}{2}. \tag{2.18}$$

Here $\Delta = g\mu_B H$ and B_S is the Brillouin function. In computing the conductance, energy-conserving δ functions relate the energies eV and Δ in the arguments of Fermi functions in Eq. (2.2). These occur in combinations

$$1 - 2f(eV \pm \Delta) = \tanh[(eV \pm \Delta)/2k_B T] , \tag{2.19}$$

corresponding physically to an inelastic threshold at $eV \pm \Delta$. The broadening of the threshold resulting from the thermal-electron energy distribution in the electrodes is included in the integral

$$H(E/k_B T) = \int_{-\infty}^{\infty} \frac{\partial}{\partial E'} f(E' - E) \tanh\left(\frac{E'}{2k_B T}\right) dE' . \tag{2.20}$$

As shown by Shen,[13] the resulting modification of $\tanh(x)$ is

$$H(x) = (-1 + e^{2x} - 2xe^x)/(1 - e^x)^2 . \tag{2.21}$$

The total conductance through second order is

$$G = G^{(1)} + G^{(2)}, \tag{2.22}$$

$$G^{(1)} = (4\pi e^2/\hbar)\rho_F^a \rho_F^b [T^2 + N_a(2TT_a + T_a^2)] , \tag{2.23}$$

$$G^{(2)} = (4\pi e^2/\hbar)\rho_F^a \rho_F^b T_J^2 N_a \{S(S+1) + \tfrac{1}{2}\langle M\rangle [H(\delta+\nu)]\} , \tag{2.24}$$

where $\nu = eV/2k_B T$, $\delta = \Delta/2k_B T$, and N_a is the density per unit area of magnetic states.

The only important third-order term[6] is of order $T_J^2 J$, and [see Eqs. (1.8)–(1.10)] is identical, apart from a scale factor, to the term discussed by Kondo.[1] The effect of magnetic field on this term has been considered in detail by Appelbaum.[6] The only intermediate states k of importance in the sum in Eq. (2.1) involve a spin flip of the local moment. Hence the Zeeman energy Δ always occurs in the energy denominator. Kondo scattering can occur with or without a spin flip between initial and final conduction-electron states, and this distinction becomes important in case $H \neq 0$. As an example, the non-spin-flip rate

$$W^{(3)}_{M,M} \propto T_J^2 M \Big\{ [S(S+1) - M(M+1)] \sum_q \frac{1 - f(\epsilon_{q-})}{\epsilon_{k+} - \epsilon_{q-} - \Delta} + [S(S+1) - M(M-1)] \sum_q \frac{f(\epsilon_{q-})}{\epsilon_{k+} - \epsilon_{q-} - \Delta} \Big\} \delta(\epsilon_k - \epsilon_k') \tag{2.25}$$

becomes

$$W^{(3)}_{M,M}(\epsilon) = -M^2 \sum_q \frac{T_J^2 J \tanh(\frac{1}{2}\beta\epsilon_{q-})}{\epsilon_{k+} - \epsilon_q - \Delta} + \cdots \tag{2.26}$$

when the bracket terms, matrix elements of $S^- S^+$ and $S^+ S^-$, corresponding to electron and hole intermediate states, respectively, are combined. We assume that T_J and J are constant in a range $-E_0 \leq \epsilon \leq E_0$ and zero elsewhere. Conversion to an integral and factoring out the energy density of states ρ_F^a gives

$$W_{M'M}(E) = -T_J^2 J M^2 \rho_F^a g(E - \Delta),$$

where

$$g(\epsilon) = P \int_{-E_0}^{E_0} \frac{\tanh(\frac{1}{2}\beta\epsilon) d\epsilon'}{\epsilon - \epsilon'} \,. \tag{2.27}$$

The major contribution to the integral $g(\epsilon)$, of course, comes near $\epsilon' = \epsilon$. As $\epsilon \to 0$, the change in sign produced by $\tanh(\frac{1}{2}\beta\epsilon)$, a step function at $\epsilon = 0$ of width $k_B T$, compensates for the change of sign in the denominator giving a logarithmic peak. Note that the magnetic field shifts the peak in $g(\epsilon)$ to $\epsilon = \Delta$. Finally, the third-order conductance is[6]

$$\begin{aligned} G^{(3)}(V,H) &= C \Big\{ 1 - \frac{\langle M^2 \rangle}{S(S+1)} + \frac{\langle M \rangle}{2S(S+1)} [H(\delta - \nu) + H(\delta + \nu)] \Big\} F(eV) \\ &+ \frac{C}{2} \Big(1 + \frac{\langle M^2 \rangle}{S(S+1)} + \frac{\langle M \rangle}{S(S+1)} H(\delta + \nu) \Big) F(eV + \Delta) \\ &+ \frac{C}{2} \Big(1 + \frac{\langle M^2 \rangle}{S(S+1)} + \frac{\langle M \rangle}{S(S+1)} H(\delta - \nu) \Big) F(eV - \Delta), \end{aligned} \tag{2.28}$$

where

$$C = (-\pi e^2/\hbar) S(S+1) \rho_F^a \rho_F^b N_a T_J^2 J,$$

and

$$F(eV) = \rho_F^a \int_{-\infty}^{\infty} \int_{-E_0}^{E_0} \frac{\tanh(\frac{1}{2}\beta\epsilon') d\epsilon'}{\epsilon - \epsilon'} \frac{\partial}{\partial \epsilon} f(\epsilon - eV) d\epsilon \,. \tag{2.29}$$

Since $(\partial/\partial\epsilon) f(\epsilon - eV)$ is sharply peaked at $\epsilon = eV$, $F(eV)$ is a slightly broadened version of $g(eV)$. Our numerical studies of this integral indicate that it is well approximated by

$$F(eV) = -\tfrac{1}{2}\rho_F^a \ln \left[\frac{(eV)^2 + (\alpha k T)^2}{E_0^2} \right], \tag{2.30}$$

with $\alpha \approx 2$, for $|eV| < E_0$.

B. Extensions of Appelbaum's Theory

We advance simple physical arguments to show that the central assumption of an exchange coupling $H^x = -2J\vec{S} \cdot \vec{\sigma}$ has further consequences observable in the tunneling experiment. These are the g shift $\Delta g = 2J\rho_F$, to first order, and a related broadening of the Zeeman transition[12] of the local moment, Eq. (1.13). This width tends to quench Kondo scattering in a magnetic field[12] by cutting off the singular function $g(\epsilon)$ for ϵ and $k_B T$ less than Γ.

The Anderson model of a localized magnetic state,[7,19] as we will see, indicates that $-J\rho_F$ need be no smaller than 0.25. There is thus no *a priori* reason to assume that these effects are small; in a sense they occur to the same order as the anomalous scattering.

The spin-flip threshold $g\mu_B H = |eV|$ in $G^{(2)}$ reveals the Zeeman excitation energy of the local moment *as it is coupled* by H^x, Eq. (1.1), to the conduction electrons in the adjacent electrode. Thus we take as spin Hamiltonian for the local moment

$$H_l = -g_0 \mu_B \vec{S} \cdot \vec{H} - 2J \sum_i \vec{S} \cdot \vec{\sigma} \,. \tag{2.31}$$

Here g_0 is the g value for the local moment in the absence of exchange coupling J. The conduction-electron spins $\vec{\sigma}$ polarize in an applied field H to produce volume spin magnetization $P = \chi_P H$, where χ_P is the Pauli susceptibility

$$\chi_P = 2\mu_B^2 \rho(E_F). \tag{2.32}$$

In this expression $\rho(\epsilon_F)$ is the density of states of one spin index at the Fermi surface. The sum in the second term in (2.31), on the assumption that the spins σ_i are in thermal equilibrium, equals $S_z \chi_P H/\mu_B$. Collecting coefficients of H and using (2.32), one finds

$$g = g_0 + 2J\rho_F^a \,. \tag{2.33}$$

Thus a negative g shift occurs for antiferromagnetic coupling $J < 0$. A more sophisticated calculation,[10] valid at $T = 0$, gives the relation

$$\Delta = \left[g_0 + \frac{2J\rho_F}{1 - J\rho_F \ln(g\mu_B H/E_0)} \right] \mu_B H \,. \tag{2.34}$$

Since the denominator goes to zero at $g\mu_B H = E_0 \times e^{1/J\rho_F} = k_B T_k$, Eq. (2.34) is valid only for $g\mu_B H > kT_K$. If the log term in the denominator is negligible, a g value is defined and Eq. (2.34) reduces to the first-order formula (2.33).

The g shift is a consequence of the diagonal elements $JS_z(a^\dagger_{k+}a_{k'+} - a^\dagger_{k-}a_{k'-})$ of the exchange interaction (2.14). The remaining terms, $J[S^+(a^\dagger_{k-}a_{k'+}) + S^-(a^\dagger_{k+}a_{k'-})]$, produce mutual spin-flip transitions of the local moment and a conduction electron. This broadens the Zeeman transition of the local moment, and permits rapid energy exchange between the local moment and a conduction electron. Since we assume that the conduction-electron spins remain in thermal equilibrium, a short spin-lattice relaxation time T_1 for the local moment is assured.

The physics is especially clear in the limit $g\mu_B H \gg k_B T$ when negligibly few conduction electrons are available with energy sufficient to excite the local moment; hence its lower spin level remains sharp. On the other hand, electrons in an energy interval $0 \geq \epsilon \geq -g\mu_B H$ of the spin-up conduction band, as shown in Fig. 3, can accept energy $g\mu_B H$ from the local moment. The corresponding deexcitation rate[9,10]

$$1/T_1 = (\pi/\hbar)(J\rho_F)^2 g\mu_B H = \Gamma/\hbar \qquad (2.35)$$

is thus proportional to $g\mu_B H$, and is by definition[9] the inverse of the spin-lattice relaxation time T_1. Here no distinction appears between level broadening $\hbar/T_2$, strictly the imaginary part of a self-energy,[10] and $\hbar/T_1$, lifetime broadening produced by the relaxation process,[9] both of which result from off-digonal elements of H^x. A clear discussion of this is given by Walker.[9] Simply replacing $k_B T$ by $g\mu_B H$ in the Korringa formula of NMR for $\hbar/T_1$ gives a result which differs from Eq. (2.35) by a numerical factor[10] of 4. This implies an energy width $\hbar/T_1$ four times larger than is directly observed in the experiment. We conclude that this extrapolation of the usual result[10] must be an overestimate, and that the correct answer for $g\mu_B H \gg k_B T$ is $\Gamma = \hbar/T_2 = \hbar/T_1$ as given by Eq. (2.35). This situation may reflect the fact that for $k_B T \gg g\mu_B H$ both excitation and deexcitation of the local moment can occur via conduction electrons. For $k_B T \gg g\mu_B H$, fluctuations in the local density of conduction electrons can contribute to Γ by modulating the resonance frequency through the coupling J. Walker[9] gives in this case

$$\Gamma = \tfrac{7}{2}\,\pi(J\rho_F)^2 k_B T\,. \qquad (2.36)$$

Higher-order corrections involving $J\rho_F \ln(g\mu_B H/E_0)$ have been given[9,10]; as in the case of the g shift, such corrections should be important only near T_K.

The above discussion is based on the s-d exchange model. The local moments in the experiment are more precisely described by the Anderson Hamiltonian,[7] which is equivalent to the s-d exchange Hamiltonian only for small $J\rho_F$.[19] It is possible that effects peculiar to the Anderson model are important for $J\rho_F \sim 0.5$. To our knowledge, predictions of g values and broadenings for the Anderson model are not available, although a recently introduced theoretical scheme[20] may permit these predictions. Such Anderson model effects may be more important than the logarithmic corrections (above) to g and Γ.

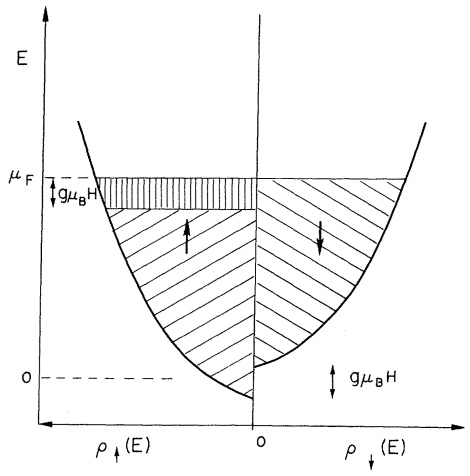

FIG. 3. Shift of spin sub-bands in a magnetic field, which leads to Pauli-spin paramagnetism. Note that in text $E = 0$ usually denotes Fermi level.

We have seen that a lifetime broadening Γ [Eq. (2.35)] is an inherent feature of the Zeeman transition of the exchange-coupled local moment for $\Delta \gg k_B T$. This broadening thus occurs in the spin-flipped intermediate states important in Kondo scattering. One can see that an energy uncertainty Γ entering the denominator of the integral

$$G(\epsilon) = \int_{-E_0}^{E_0} [\tanh(\tfrac{1}{2}\beta\epsilon')/(\epsilon - \epsilon')]d\epsilon' \qquad (2.37)$$

will cut off the peak of $g(\epsilon)$ at $\epsilon = 0$. Suhl has pointed out[21] that the appropriate treatment of a distribution $R(\epsilon)$ of intermediate-state energies is to replace everywhere $\tanh(\frac{1}{2}\beta\epsilon)$ by the convolution

$$S(\epsilon) \equiv \int_{-\infty}^{\infty} R(\epsilon')\tanh[\tfrac{1}{2}\beta(\epsilon - \epsilon')]\,d\epsilon' \qquad (2.38)$$

as in $g(\epsilon)$ and $F(eV)$. The distribution appropriate to lifetime broadening is the Lorentzian

$$R(\epsilon) = (\Gamma/\pi)/(\Gamma^2 + \epsilon'^2)\,. \qquad (2.39)$$

In the limit $\Gamma \gg k_B T$, it is easy to find that

$$S(\epsilon) \approx (2/\pi)\tan^{-1}(\epsilon/\Gamma)\,. \qquad (2.40)$$

Since this function is again a step at $\epsilon = 0$, but with step width $\sim \Gamma$ instead of width $\sim k_B T$, one expects that

$$g(\epsilon) \approx -\tfrac{1}{2}\ln[(\epsilon^2+\Gamma^2)/E_0^2] \ . \qquad (2.41)$$

The peak $g(0)$ is thus reduced from $-\log(k_BT)$ to $-\log\Gamma$. Our point of view is that any mechanism leading to an energy width in the transition to the spin-flipped intermediate state will reduce the peak. In magnetic resonance parlance, the resonance width $\hbar/T_2$, is what counts. This is consistent with Suhl's example of dipole-dipole coupling,[21] which does not contribute to the spin-lattice relaxation rate $\hbar/T_1$, but nevertheless gives an energy width and quenches the Kondo scattering. A different mechanism has been proposed by other workers,[22] who argue that, since Kondo scattering may be regarded as an interference between two scattering amplitudes, a short coherence time should reduce the resonant scattering rate. The available coherence time is limited by T_1, the spin-lattice lifetime of the local moment. In our experiment at high field, since $T_1 = T_2$, the two mechanisms are coincident. In other situations, as in Suhl's example,[21] one may more readily distinguish the two mechanisms. The broadening is included in the $G^{(2)}$ terms by similarly convoluting the $H(x)$ function representing the inelastic threshold for Zeeman excitation. Thus we replace $H(x)$ defined in Eq. (2.21) by

$$\overline{H}(x) = \int_{-\infty}^{\infty} \frac{\Gamma}{\pi} \frac{H(x-y)}{\Gamma^2+y^2}\, dy \qquad (2.42)$$

in the $G^{(2)}$ conductance, Eq. (2.24). The $G^{(3)}$ equations (2.28) and (2.29) should be modified by replacing $\overline{H}(x)$ and by replacing $\tanh(\frac{1}{2}\beta\epsilon)$ by $S(\epsilon)$ in (2.29).

It is worthwhile to compare the tunneling experiment with the conventional ESR experiment in measuring the Zeeman transition of a local moment. As we have seen, the derivative d^2I/dV^2 reveals the Zeeman spectrum of the local moment; the conduction electrons are evident only through the negative g shift. In an ESR experiment, on the other hand, absorption from the microwave magnetic field $H_1\cos\omega t$ occurs by the local moment *and* the conduction electrons. A necessary condition for separating the contributions of the local moments and the conduction electrons is that their respective g values differ substantially. However, this is often not the case, for strong exchange coupling between the conduction electrons and the local moments can give a motional averaging effect so that only one resonance is observed. One can see what is involved in this case by imagining that the resonant frequency of a particular electron spin jumps back and forth randomly between values $g_0\mu_BH/\hbar$ and $g_e\mu_BH/\hbar$ as the electron by diffusion and the exchange mechanism spends some time in the conduction band and some time bound as a local moment. If the rate ω_D, at which the frequency changes occur, exceeds the spin-lattice relaxation rate $1/T_1$ and becomes comparable to the frequency difference $\Delta\omega = (g_0 - g_e)\mu_BH/\hbar$, the two resonances merge. In the limit of $\omega_D \gg \Delta\omega$, the g value of the resultant motionally narrowed resonance depends on g_0, g_e, and on the relative concentrations of conduction electrons and local moments. It is for this reason that large first-order g shifts are not observed in ESR measurements[23] on dilute magnetic alloys.

In the foregoing discussion we assume $\omega_D \gg 1/T_1$; thus the conduction-electron spins are more tightly coupled to the local moments than to the lattice. Hence they are not necessarily in thermal equilibrium. In the tunnel junction, on the other hand, an estimate shows that thermal equilibrium is maintained by the conduction-electron spin system. In addition, the local moments in the ESR case are excited coherently by an applied microwave field, while in the tunnel junction there is no reason to assume coherence between spin-flip transitions produced by electrons tunneling at different places over the area of the junction.

In summary, the tunneling experiment directly probes the energy, temperature, and magnetic field dependence of the scattering rate W_{ij} produced by the exchange coupling H^x by measuring the additional current through the barrier. The $eV = 0$ limit of the anomalous conductance corresponds directly to the incremental resistivity produced by exchange scattering W_{ij} in the usual bulk measurements; in fact, the same Kondo integral occurs in both contexts. Comparison of the added tunnel conductance at $V = 0$ to the incremental resistivity predicted by the nonperturbative theories[2-5] of exchange scattering is also appropriate. The magnetic susceptibility of the local moment bears the same relation to the anomalous conductance as it does to the incremental resistivity in bulk measurements.

C. Schottky-Barrier Tunnel Junctions

Group-IV semiconductor surfaces exhibit a density of surface states strongly peaked in the lower portion of the forbidden gap.[24,25] Equilibrium of an N-type semiconductor-vacuum interface is achieved by partial filling of these states with electrons removed from donors in a region near the surface. This typically locates the surface Fermi level at a point approximately $\frac{1}{3}E_g$ above the valence-band edge at the zone center. For an N-type sample as shown in Fig. 2, the conduction-band edge thus bends up by $eV_B \approx \frac{2}{3}E_g$ to form a barrier of height eV_B for conduction electrons. Since $eV_B \gg k_BT$, most of the barrier region is totally depleted of extrinsic electrons. If follows from Poisson's equation, assuming random distribution of donor ions, that the variation of the conduction-

band edge with position, taking $z=0$ at the surface, is

$$V(z)=V_B(z-z_0)^2/z_0^2\,, \tag{2.43}$$

where the depletion layer depth z_0 is[26]

$$z_0=[\epsilon(eV_B+\mu_F)/2\pi N_D e^2]^{1/2}\,. \tag{2.44}$$

Here ϵ, μ_F, and N_D are the dielectric constant, Fermi degeneracy, and donor concentration, respectively. The parabolic dependence [Eq. (2.43)] is inaccurate near the inner edge of the region where free charge occurs with consequent screening. Since the barrier is low in this region, the appropriate modification to an approximate exponential variation is unimportant in determining tunneling probabilities.[26] In an intimate metallic contact to a group-IV semiconductor, the above features are nearly unchanged.[24,25] The surface states overlap strongly with the metallic conduction states and are presumably delocalized. The depletion layer depth z_0 is typically ~ 100 Å, much larger than an dipole layer in the metal, which can thus be neglected. The Schottky barrier appropriate to the present studies is shown in Fig. 3.

The tunnel conductance of the parabolic barrier model which is suggested by the above has been calculated exactly by Conley, Duke, Mahan, and Tiemann[16] (CDMT) by matching wave functions at the boundaries $z=0$ and $z=z_0$. The barrier transmission factor $|T|^2$ is directly obtained from the ratio of $|\Psi|^2$ on the opposite sides of the barrier. The assumed wave functions in the semiconductor bulk and in the metal are effective-mass states, while the eigenfunctions in the barrier region, characterized by the potential (2.43), are parabolic cylinder functions. The latter functions neglect mixing[26] of valence-band states in the barrier; hence the procedure is most accurate for $eV<\frac{1}{2}E_g$.

An important feature in determining the conductance spectrum $G(V)$ is that the applied voltage V influences the barrier transmission by varying the barrier thickness through the relation

$$z_0=[\epsilon_0(eV_B+\mu_F-eV)/2\pi N_D e^2]^{1/2}\,. \tag{2.45}$$

The conductance increases approximately as

$$G(V)\sim e^{eV/E_1}\,x\,e^{-eV_B/E_1} \tag{2.46}$$

for large positive bias, corresponding to electron flow into the metal as a result of the decrease of z_0 with V. The parameter E_1,

$$E_1=[\pi N_D e^{2*}\hbar^2/m\epsilon_0]^{1/2}=\tfrac{1}{2}\hbar\omega_p\,, \tag{2.47}$$

is 42.4 meV for Si: (1.6×10^{19} cm^{-3} P). Note that for increase of positive-bias voltage beyond μ_F/e, there is no corresponding increase in the number of semiconductor electrons able to tunnel into the metal. If $\mu_F<E_1$, so that the barrier transmission is slowly increasing with bias, this consideration leads to a minimum in the conductance at $eV=\mu_F$. Although the above discussion assumes the conduction band of the semiconductor is centered at $k=0$, this restriction is not essential.[16,27] Since the Fermi wave vector k_F in the metal is larger than the displacement k_0 in k space of a band minimum in the semiconductor, direct tunneling transitions can occur.

In this case the criterion for neglecting band mixing, $eV_B\leq\frac{1}{2}E_g$, is to be evaluated with $E_g(k_0)$; in Si, $E_g(k_0)$ is ~ 4.5 eV. The generalization[27] to a nonspherical conduction band has also been carried out and leads to only minor changes in the predicted characteristics.

The CDMT model is most successful in a range of semiconductor doping N_D sufficiently large that two-step real-intermediate-state tunneling[28] is unimportant, and small enough that the actual barrier potential is well approximated by the average potential V(z). In the high-concentration (thin-barrier) limit, statistical fluctuations in the number of ions in the barrier region make the average potential less accurate. A figure of merit in this regard is $\bar{n}=z_0^3N_D\propto N_D^{-1/2}$, the number of ions contained in an area z_0^2 of the barrier. If $\bar{n}$ is small, its relative fluctuations $\Delta n(\vec{r})/\bar{n}$ from point to point along the barrier will be greater.

Since it is known experimentally that the barrier height V_B is independent of donor concentration N_D, we neglect fluctuations in V_B and assume that fluctuations in the local density of ions in the barrier cause fluctuations only in the barrier thickness z_0 and consequently in the parameter E_1, (2.47). The importance of such fluctuations in E_1 on the tunneling conductance arises from the exponential dependence $G\propto e^{-eV_B/E_1}$, with $eV_B\gg E_1$, which strongly weights the fluctuations in the direction of increased conductance.

We make a simple estimate of the conductance increase the fluctuations afford. We imagine the barrier divided up into units of area z_0^2, and sum the conductances due to each of the small units. We assume that the probability of finding n ions in a unit is given by the Poisson distribution

$$P(n,\bar{n})=(\bar{n})^n e^{-\bar{n}}/n!\,.$$

Then the barrier fluctuation factor is

$$\frac{G(\bar{n})}{G(\infty)}=\sum_{n=0}^{\infty}P(n,\bar{n})\exp[-(eV_B/E_1)(\bar{n}/n)^{1/2}]/\exp(-eV_B/E_1)\,. \tag{2.48}$$

Evaluated for Si:(1.6×10^{19} cm^{-3} P), with $\bar{n}=9.4$ for $z_0=84$ Å, $eV_B=0.85$ eV, and $eV_B/E_1=20$, the barrier fluctuation factor is 11.7, with the current flowing dominantly through units with $n=15$. On the other hand, for the case of the Pb/Ge: (7.5×10^{18}

cm^{-3} Sb) junctions for which agreement with the CDMT model has been previously reported,[17] we estimate the factor as 2.2. The larger value $\bar{n} = 13.7$ and smaller exponent $eV_B/E_1 = 18.2$ in Ge both reduce the importance of fluctuations.

While it is clear that the appropriate size of the sampling volume is near z_0^3, this may not be precise and consequently the factor quoted for Si is probably uncertain by a factor of 2.

D. Localized Magnetic Moments in Schottky Barriers

Experimental evidence[11] indicates that localized moments are generally present in Schottky barriers with doping N_D not greatly exceeding the Mott concentration N_c, that these are located at the inner edge of the depletion region, and that their characteristics depend on the chemical species[12] and concentration of the donors. We argue that the formation of a thin layer of transiently localized states, well described by the Anderson model[7] and resembling donor states, is indeed plausible. The expected resemblance to the well-studied donors permits additional estimates of the local moment properties. For example, the g values of noninteracting donors are generally known, and in Si are close to 2.0. In addition, electron scattering experiments[29,30] on P donors in Si directly indicate an antiferromagnetic exchange coupling between the donor and a conduction electron. The total singlet spin-exchange cross section for the P donor is measured to be [31] $\sigma_x \cong 2\times10^{-12}$ cm^2.

In the idealized Schottky-barrier model described above, the free carrier density is assumed to rise continuously from zero at the inner edge of the depletion layer to N_D in the bulk. This variation occurs over a distance of the order of the Fermi-Thomas screening length λ [26]:

$$\lambda = [\epsilon \mu_F / 6\pi N_D e^2]^{1/2} , \qquad (2.49)$$

which is ~10 Å at $N_D \cong 10^{19}$ cm^{-3}. On the other hand, one may argue that near z_0, where the electron concentration is less than the Mott critical concentration N_c,[32] such that $\lambda(N_c) \geq a_0^*$, the effective Bohr radius, those electrons present may tend to localize. N_c for P donors in Si is 4×10^{18} cm^{-3}, and somewhat larger for As donors. Indeed, as the concentration N_D is reduced toward N_c, electron localization occurs throughout the semiconductor crystal. Near the inner edge of the depletion region the screening may be sufficiently reduced, even for N_D several times N_c, that localized electron states can appear, as indicated in Fig. 4(a).

This situation is described more precisely by the Anderson Hamiltonian[7,33] for a single localized state "ϕ_d," interacting with a set of conduction states:

$$H = \sum_k \epsilon_k n_k + \sum \epsilon_d n_d + U n_{d\uparrow} n_{d\downarrow}$$

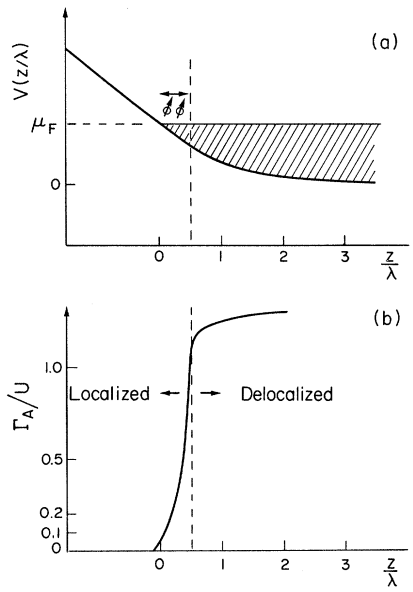

FIG. 4. (a) Location of moments at inner edge of depletion region. Band edge varies as $e^{-z/\lambda}$, where λ is Fermi-Thomas screening length. Vertical dashed line corresponds to free-electron density of the Mott critical concentration N_c, and separates region of localized states, on left, from region of delocalized states, on right. (b) Highly schematic plot of Γ_A/U in the Anderson model versus position z in the semiconductor. Γ_A/U must be near zero in the depletion layer and exceed unity in the degenerate bulk. $\Gamma_A/U \approx 1$ corresponds to the Mott transition; local moments with $J\rho_F = -(8/\pi) \times \Gamma_A/U$ occur where $\Gamma_A/U \leq 0.1$.

$$+\sum_k (V_{kd} c_k^\dagger c_d + V_{kd} c_d^\dagger c_k) . \qquad (2.50)$$

Here U is the Coulomb (repulsive) energy of a second electron of opposite spin on the same site and V_{kd} is a one-electron energy describing the mixing of localized and free states. The energy $\epsilon_d < 0$ is the one-electron level measured from the Fermi level. The V_{kd} term produces a broadening

$$\Gamma_A = \pi |V_{kd}|^2 \rho_F \qquad (2.51)$$

of the localized one- and two-electron levels ϵ_d and $\epsilon_d + U$, respectively, which results from a second electron hopping on and off. Γ_A in the Hubbard[34] and Anderson[7] models plays the role of screening the Mott description,[32] and the ratio Γ_A/U describes the effective-interaction strength. At $\Gamma_A/U \lesssim 0.1$, the state is localized and magnetic[7]; for $\Gamma_A/U \gtrsim 1.0$, the state is delocalized.[7,33] The latter condition also corresponds to the Mott delocalization criterion.[34] Quite possibly values of Γ_A/U greater than 0.1 but less than 1.0 are still localized. If we refer again to the Schottky barrier [Fig. 4(b)] evidently Γ_A/U is large in the bulk region and near zero in the depletion region; we

may expect localized states near the inner edge of the depletion region where $\Gamma_A/U \sim 0.1$.

It has been shown[19] that for $\Gamma_A/U \ll 1$, the Anderson Hamiltonian can be transformed to remove the V_{kd} term and to include the s-d exchange interaction of Kondo,[1] Eqs. (1.1) and (2.14), where J is antiferromagnetic and has an explicit energy dependence[19]:

$$J(\epsilon) = -2|V_{kd}|^2\left[\frac{1}{\epsilon-\epsilon_d} - \frac{1}{\epsilon-(\epsilon_d+U)}\right] . \quad (2.52)$$

Note that $-J(\epsilon)$ has a minimum value at $\epsilon = 0$, which is

$$J(0) = 2|V_{kd}|^2 U^2/\epsilon_d(\epsilon_d+U) .$$

In the symmetric case $\epsilon_d = -\frac{1}{2}U$, by combining Eq. (2.52) with Γ_A of Eq. (2.51), one obtains

$$J\rho_F = (-8/\pi)(\Gamma_A/U) . \quad (2.53)$$

Anderson's estimate[7] $\Gamma_A/U \cong 0.1$ thus directly implies from (2.53) $J\rho_F \approx -0.25$, i.e., a first-order g shift $\Delta g = 2J\rho_F \approx -0.5$. Although (2.53) is strictly valid only for $\Gamma_A/U \ll 1$, it is likely that larger values of $-J\rho_F$ will occur as Γ_A/U increases from 0.1 to ~ 1.0, going to the right in Fig. 4(b), before the state becomes delocalized.

An upper limit on the width of the layer in which such localized donor moments may form is given by the screening length λ. As N_D is increased, we expect a correspondingly thinner layer and that the moments will have a stronger exchange coupling, Eq. (2.53). It is probable that for much larger N_D no localization will occur. The experimental results, however, do indicate localized moments in the case of P donors in Si at $N_D = 1.6\times10^{19}$ cm^{-3}, or $N_D \approx 4N_c$.

In the limit of weak coupling $\Gamma_A/U \to 0$, the donor state provides a microscopic model of the local moment. The most important parameter that such a model provides is g_0, the g value in the absence of exchange coupling. For dilute donors in bulk Si, g_0 values[31] are extremely close to 2.0. In the case of interacting donors, we may ask if other sources of g shift, apart from the exchange effect above, will be important. One possible source of other g shifts would be electric fields produced by ionized donors. The wave function of the state may thus be distorted, but it seems unlikely that any orbital angular momentum could be mixed into the s-like donor ground state because of the low symmetry of the local electric fields. We conclude that $g_0 = 2$ is likely to be preserved.

The binding energy of the P donor in Si is 45 meV and the Bohr radius $a_0^* = 20$ Å.[32] Small concentrations of conduction electrons drastically reduce the spin-lattice relaxation time T_1 of the donor ESR in low-concentration samples. Analysis of this effect[35] enabled Feher and Gere[31] to determine the cross section σ_x of the donor for spin exchange with a free electron. The measured value $\sigma_x = 2\times10^{-12}$ cm^2 is extremely large, and remarkably close to that obtained by scaling (for the mass m^* and dielectric constant ϵ_0) the hydrogen-atom estimate due to Oppenheimer: $\sigma_x = \pi(12a_0^*)^2$, which gives $\sigma_x = 3\times10^{-12}$ cm^2. ESR measurements[31] on samples containing more than 3×10^{18} cm^{-3} donors show a narrow resonance characteristic of free electrons. The conduction-electron spin-lattice relaxation time T_1 deduced from the width of this resonance is 3×10^{-7} sec.[31]

Elegant electron scattering experiments on P donors in Si have been performed recently by Honig,[29,30] employing low temperatures (0.3 °K) and a magnetic field in order to achieve spin polarization of the interacting donors. Honig concludes that the zero-energy cross section for singlet scattering $4\pi A_s^2$ (donor and conduction-electron spins antiparallel) exceeds the triplet cross section $4\pi A_t^2$ by a factor of 4.8, close to that predicted for the hydrogen atom. It is possible further to deduce that the singlet scattering length A_t is negative, while A_s is positive. Honig concludes that the singlet P negative-ion state is bound, while a virtual triplet state occurs in the continuum.[30] Note that the singlet state is precisely the doubly occupied state of the Anderson model. His experiments thus confirm that the exchange interaction is antiferromagnetic, in agreement with the Anderson model.

An estimate of N_A, the number of local moments per unit area, can be made on the assumption that, where the local electron density falls below N_c, all electrons are localized.[32] This criterion appears to be most valid for $N_D \geq N_c$, and probably overestimates N_A for $N_D \gg N_c$. The conduction-band edge [see Fig. 4(a)] variation near the boundary of the depletion region and the degenerate region is taken[26] as

$$V(z) = \mu_F e^{-z/\lambda} . \quad (2.54)$$

Here λ is the screening length and now we take $z = 0$ at the crossing of the Fermi level and the conduction-band edge, and $V = 0$ at the bottom of the conduction band.

The local carrier density corresponding to (2.54) is

$$n(z) = N_D(1 - e^{z/\lambda})^{+3/2} . \quad (2.55)$$

In the region of interest, for $N_D = 1.6\times10^{19}$ cm^{-3} and $N_c = 4\times10^{18}$ cm^{-3}, we have $n(z)/N_D \leq \frac{1}{4}$. Hence the local Mott transition occurs at $z = z_c$, where $z_c = 0.5\lambda$. It is thus reasonable to expand the exponential and retain only the linear term. Equation (2.55) reduces to

$$n(z) \approx N_D(z/\lambda)^{3/2} ,$$

which gives

$$z_c \approx \lambda (N_c/N_D)^{2/3} . \quad (2.56)$$

The number of moments per unit area, N_A, is

$$N_A = \int_0^{z_c} n(z)\,dz \cong \tfrac{2}{5} N_D \lambda (N_c/N_D)^{5/3} . \quad (2.57)$$

Taking $N_D = 1.6\times10^{19}$ cm^{-3}, $\lambda = 10$ Å, and $N_c = 4\times10^{18}$ cm^{-3}, we estimate $N_A \approx 0.6\times10^{11}$ cm^{-2}. As we will see below, this is remarkably close to the estimate based on the measured spin-flip conductance and the donor spin-exchange cross section.

III. EXPERIMENTAL METHODS

We now turn to the experimental techniques used in fabricating Schottky-barrier tunnel junctions on single crystals of degenerate semiconductor, and in measuring the exchange-tunneling component of the differential conductance $G(V)$ and its derivative $(d/dV)G(V)$. We have made these measurements at temperatures down to 1.3 °K and in magnetic fields up to 150 kOe.

A. Samples

Single crystals of Si containing P and As were obtained from the Monsanto Chemical Co. in the form of Czochralski boules about 1 in. in diameter, with ⟨111⟩ axes. Disks 1 mm thick were cut to provide spiders for Hall measurements. Disks 10 mm thick were cut and sliced into bars $2\times4\times10$ mm^3, with ⟨111⟩ normal to the 2×4-mm^2 face, for the tunnel junctions. Two low-resistance contacts were provided on each bar by alloying gold in a hydrogen atmosphere (800 °C for 15 min). Chemical analysis of the silicon for trace impurities by semiquantitative emission and spark source mass spectrographic techniques showed transition-metal impurity levels below 1 ppm.

Hall and resistivity measurements on spiders cut from slices adjacent to the tunneling samples were made at 300, 77, and 4.2 °K. Measured values on Si: P of ρ and $N_D = 1/Re$ at 300 °K were 0.0043 Ω cm and 1.6×10^{19} cm^{-3}, in agreement with the nominal values. The temperature dependence agrees with that reported elsewhere[36] for similar degenerate samples. Magnetoresistance measurements with $\vec{H} \perp \vec{I}$ on Hall samples of Si: (1.6×10^{19} cm^{-3} P) give $\Delta\rho/\rho \approx -0.2\%$ at 3 kOe and $\Delta\rho/\rho \approx +2\%$ at 132 kOe at 1.3 °K.[37]

B. Junction Fabrication

The tunnel junction consists of an evaporated metal dot on a ⟨111⟩ cleavage plane of the crystal. A sample is illustrated in Fig. 5, along with its equivalent circuit. The intention in junction fabrication is to exclude chemical constituents other than the degenerate semiconductor and the electrode metal. This ideal is approached by cleaving the semiconductor in a high-vacuum chamber *during* a rapid evaporation of the desired electrode metal. The fixture used has been described elsewhere.[15] Cleavage and positioning of a light stainless-steel screen, which contains an array of 0.02-cm-diam. holes and is lightly spring loaded against the semiconductor bar, take ~0.02 sec. The pressure during evaporation is ≤ 10^{-6} Torr, so that the monolayer time is of the order of 1 sec. The evaporation rates are as high as convenient, typically 10–40 Å/sec. These considerations indicate that, although the electrode metal may conceivably have a few-percent residual gas contamination, there is no intervening layer between this metal and the silicon. Prior to being mounted in the evaporator, two gold Ohmic contacts (< 0.5 Ω) were alloyed onto each bar sample. Fine copper wires were then soldered to the gold, so that it would not be necessary to heat the sample after the cleavage. The result of vacuum cleavage of a $2\times4\times10$-mm^3 silicon bar is a 2×4-mm^2 face with an array of metal dots. The faces are generally rough with small areas of perfect ⟨111⟩ cleavage plane.[38] It is usually possible to find several dots situated on such an area, and only such metal dots are contacted in tunneling measurements.

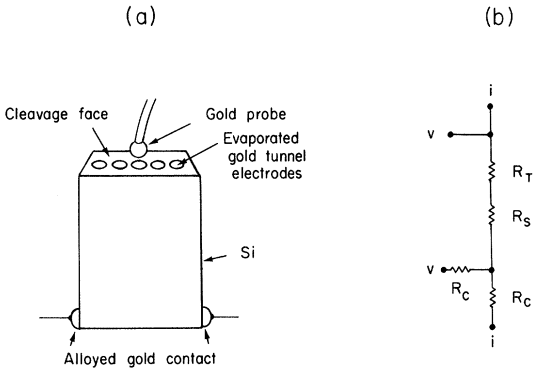

FIG. 5. (a) Tunnel junction on single-crystal silicon bar, showing evaporated metal tunnel electrodes and alloyed gold return contacts. Contact to evaporated metal electrodes is made with a lightly tensioned gold probe. ⟨111⟩ direction in the silicon bar is vertical. (b) Equivalent circuit of tunnel samples. R_T, R_s, and R_c represent the tunnel junction dynamic resistance dV/dI, the spreading resistance, and the alloyed contact resistance, respectively. Current and voltage terminals are labeled i and v. R_s is negligible in samples studied.

The dots are 1000–5000 Å thick. Contact to a dot is established with a clean gold probe gently tensioned against the dot. The gold probe is ~0.015 in. in diameter, formed by melting the end of an 0.008-in.-diam gold wire in an oxygen gas flame. Every effort is made to keep the gold probe and the evaporated dot clean before contact is

established. The samples were stored and transported in a vacuum desiccator, and showed no change in properties during a month.

Important advantages of this procedure are that the temperature of the junction is never raised above 300 °K, giving no reason to expect a redistribution of dopant atoms near the interface, and that no chemicals are allowed to come into contact with the semiconductor surface or the evaporated metal film.

As indicated in Fig. 5, the tunneling sample allows a 4-terminal measurement of the Schottky-barrier junction to the extent that the spreading resistance R_s is negligible. This series resistance arises from constriction of the current-flow lines in the semiconductor into the small area of the evaporated dot, and is given by $R_s = \rho/2d$. Evaluated for diameter $d = 0.02$ cm and resistivity $\rho \approx 0.0015$ Ω cm at 4.2 °K, we find $R_s \approx 0.04$ Ω or $\sim \frac{1}{2}\%$ of the junction resistance R_T, which we can neglect. This conclusion is confirmed empirically by observation of prominent Si phonons at the correct bias energies and, more importantly, by the absence of any shift in these phonon positions at 150 kOe. We can thus rule out distortion from any bulk magnetoresistance effect.

C. Harmonic Derivative Measurements

Standard methods[39] were used to measure dV/dI and d^2V/dI^2 of the tunnel junctions as a function of applied bias V. The circuit and instrumentation

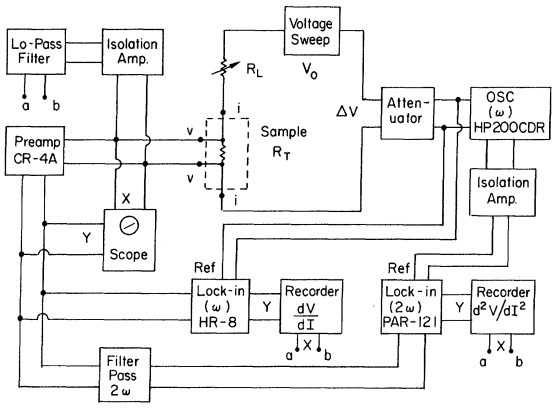

Fig. 6. Instrumentation for simultaneous recording of dV/dI and d^2V/dI^2. [See also Fig. 5(b).] Selector switch, not shown, permits study of two tunnel junctions, of the series resistance of the two return contacts (R_c) on each junction, and also allows substitution of a precision resistance box for calibration. Isolation amplifiers are Neff wide-band dc units and the low-pass filter has a cutoff at 1 Hz. PAR model 121 lock-in has an internal frequency doubler in the reference channel. Sample is immersed in liquid helium in a metal Dewar positioned in the Bitter electromagnet.

are indicated in Fig. 6. Measurement of voltage derivatives, rather than the more physically significant current derivatives, is advantageous when it is important to minimize possible distortion arising from non-negligible return contact resistance. In the junctions studied, the tunneling resistance $R_T = dV/dI$ is typically 10–20 Ω and the current and voltage contact resistances $R_c \sim 1\Omega$. However, the return contacts usually were somewhat non-Ohmic at 4.2 °K, and occasionally R_c increased to several ohms at 150 kOe. In the circuit shown in Fig. 6, errors in measuring the junction voltage V arising from the contact resistance R_c appear as R_c/R_i where the amplifier input impedance R_i is at least 20 000 Ω, and are thus entirely negiligible. The ac signal voltage $S(t)$ appearing across the potential terminals of the tunneling sample is

$$S(t) = \frac{dV}{dI}\frac{\Delta V \cos\omega t}{R_L + R_T + R_c} + \frac{1}{2}\frac{d^2V}{dI^2}\left(\frac{\Delta V}{R_L + R_T + R_c}\right)^2 \frac{\cos 2\omega t}{2} + \cdots \quad (3.1)$$

and the source impedance is $R_T + R_c$. The signals referred to as dV/dI and d^2V/dI^2, detected synchronously and plotted, are actually the coefficients of $\cos\omega t$ and $\cos 2\omega t$ from this expression. It is evident that voltage or magnetic field variation in R_T and R_c introduces distortion of order $(\Delta R_T + \Delta R_c)/R_L$ in dV/dI and twice that in d^2V/dI^2. These errors are reduced to a negligible magnitude by our standard choice of $R_L = 100R_T$. The HP-200-CDR low-distortion oscillator (see Fig. 6) was normally set at 2500 Hz. The PAR CR-4A preamplifier (input impedance 20 kΩ) was normally operated at a gain of 10. Its output was fed to a PAR HR-8 lock-in to detect the ω component, and through a band-pass filter (UTC BPM 5000) peaked at 5000 Hz to the PAR model 121 lock-in to detect the 2ω component. Calibration of the dV/dI charts and location of the zero of d^2V/dI^2 were accomplished by substituting a precision resistance decade box for the tunnel sample. To avoid distortion of structure in dV/dI versus V, the peak-to-peak value of the ac voltage $S(t)$ was maintained below 0.3 mV at high field, below 0.1 mV at zero field above 1 °K, and at 0.005 mV in the zero-field measurement extended below 1 °K.[40]

D. Measurements at High Magnetic Field

After adjustment of the gold probe contact and testing of the junction characteristics at room temperature, the sample was slowly immersed, without precooling, in liquid helium, contained in a metal immersion Dewar. The Dewar was then located with its tail section in the $2\frac{1}{8}$-in. air bore of a Bitter electromagnet capable of generating an

axial magnetic field of 150 kOe. Normally, the field H was parallel to the direction of tunneling. Study of a transversely oriented sample gave identical results. Cooling below 4.2 °K was accomplished by pumping on the liquid helium. The temperature of the immersed junction was determined from the helium vapor pressure (1958 scale) as measured by Wallace and Tiernan gauges, type FA-160.

Two difficulties were encountered, which were specifically associated with the high magnetic field. The first was inductive pickup in the voltage leads due to residual low-frequency ripple on the field and to vibration of a loop formed by the potential leads in a fixed field gradient. These noise voltages were monitored on an oscilloscope, and were in some instances as large as 200 μV at 150 kOe. Since neither of these signals is coherent with the applied modulation, and since neither exceeds the desired first harmonic signal, they are efficiently excluded by the phase-coherent detector and do not contribute to modulation broadening. To reduce noise on the x axis of the xy recorder set at a sensitivity of 1.0 mV/in., a low-pass filter was incorporated. The signal-to-noise ratio in dV/dI measurements was always good, and that in d^2V/dI^2 was ~10:1 with an ac signal voltage of 0.3 mV peak to peak on a 20-Ω sample.

The second difficulty, occasionally encountered, was an increase in resistance of as high as a factor of 10 in one of the alloyed gold return contacts. This behavior is not understood and was never observed in a Schottky tunnel contact. The standard practice was to display the dV/dI spectrum of the two return contacts in series at full field, and in cases of contact resistance above a few ohms to appropriately increase the value of R_L or to reject the junction.

E. Data Processing Procedures

At high field, measurements were made simultaneously of dV/dI and d^2V/dI^2. Both derivatives were recorded to permit conversion of d^2V/dI^2 to d^2I/dV^2 by the relation

$$d^2I/dV^2 = -(d^2V/dI^2)(dV/dI)^{-3} . \qquad (3.2)$$

The dV/dI charts were calibrated by substitution of a precision resistance box for the tunnel junction; dV/dI was recorded for three calibration resistances R_B to test for linearity in the measuring circuit. Substitution of R_B for the sample served also to determine the zero of d^2V/dI^2 and to verify the purity of the oscillator signal. A computer program was written to calculate dV/dI and dI/dV from the ordinate and calibration values R_B on the xy charts and to calculate d^2I/dV^2 using Eq. (3.2).

IV. EXPERIMENTAL RESULTS

A. Background Tunneling Spectrum

The zero-field dV/dI characteristic of a Schottky junction of Au on Si:P at 1.3 °K is shown in Fig. 7. This spectrum, apart from the fine structure at $V=0$ and $V=18$ mV, is independent of temperature below 4.2 °K. A similar curve, converted to conductance and plotted on a semilog scale, is shown in Fig. 8. The zero-bias resistance of such Au|Si: (1.6×10^{19} cm^{-3} P or As) junctions at 4.2 °K was always between 10 and 20 Ω; these variations, which could result from small variations in N_D, were not accompanied by changes in the voltage dependence. The dashed curve is the conductance numerically computed from the CDMT model,[16] taking parameter values $V_B = 0.85$ V, $\epsilon_0 = 11.7$, $m_\perp = 0.26m_e$, $N_D = 1.6\times10^{19}$ cm^{-3}, and $z_0 = 84$ Å, for junction area 3.1×10^{-4} cm^2, and corrected with a barrier fluctuation factor, Eq. (2.48), of 11.7. The experimental curves show a conductance minimum at 25 ± 2 mV, about 20% higher than the calculated Fermi degeneracy, $\mu_F = 21$ meV. The positive increment in conductance produced by the TA phonon at 18.3 meV may contribute slightly to this shift, and to broadening of the minimum. The conductance minimum is broader, and the conductance variation at larger positive bias less rapid, than the theory predicts. In the latter regard, comparison with the CDMT model is similar to that reported for the case of Ge.[17]

The barrier height V_B used for the comparison of Fig. 8 was determined by capacitance measurements on vacuum-cleaved Au-Si junctions with 4×10^{18} cm^{-3} P donors. Our measurements yielded the usual straight-line variation of C^{-2} versus V

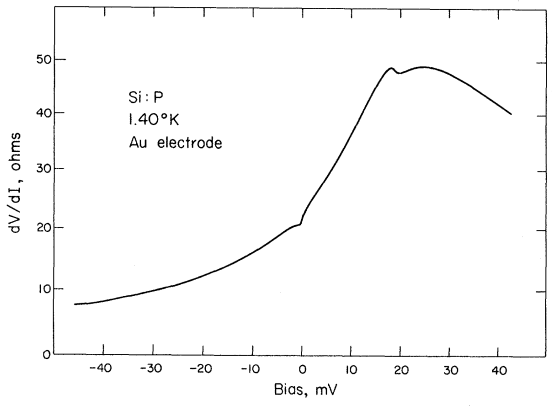

FIG. 7. Zero-field dV/dI spectrum of Au | Si:P junction at 1.4 °K. Note zero-bias conductance peak and conductance increase at 18.5 mV, corresponding to the TA phonon. Broad maximum in dV/dI near $V=25$ mV locates Fermi degeneracy of semiconductor, consistent with CDMT theory.

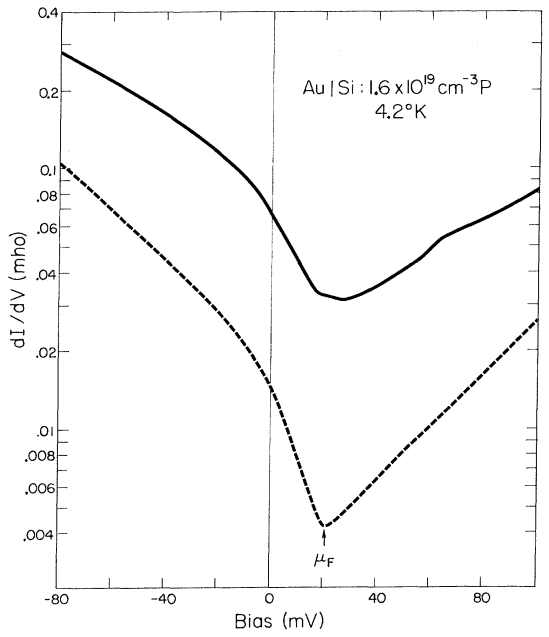

FIG. 8. Conductance, plotted on semilog scale, for typical Au junction on Si : (1.6×10^{19} cm^{-3} P). Dashed curve is CDMT theory, corrected by Eq. (2.48), corresponding to parameter values $\epsilon_0 = 11.7$, $m_\perp = 0.26$, $\mu_F = 21$ meV, $N_D = 1.6\times10^{19}$ cm^{-3}, $V_B = 0.85$ V (see text), and junction area 3.1×10^{-4} cm^2. Experimental conductance level may vary by up to ±40% in different junctions, with no change in bias dependence; calculation is accurate within a factor of ~4 (see text).

and $V_B = 0.85 \pm 0.05$ V. This result is in good agreement with previous measurements by Archer and Atalla[41] on samples with somewhat lower N_D. A direct measurement of the barrier height on samples with $N_D = 1.6\times10^{19}$ cm^{-3} has not been possible because of the difficulty in measuring the voltage variation of the capacitance on junctions with a voltage-dependent tunneling resistance as low as 10 Ω. The parameters used in the CDMT and barrier fluctuation calculations are all either directly measured or are standard values. The theoretical conductance level in Fig. 8 is approximately a factor of 4 lower than that measured. The calculated conductance, however, is very sensitive to any errors that appear in the exponential factor. Thus the error ±0.05 V in the barrier height produces an uncertainty factor of 3.2±1 in the conductance level. The estimated factor-of-2 uncertainty in the barrier fluctuation factor has been mentioned above. Finally, a 10% error in the donor concentration would lead also to a factor-of-2 uncertainty. For these reasons, we consider the comparison of experimental conductance level and the extended CDMT theory to be satisfactory. The discussion of Eq. (2.48) concludes that small areas of the barrier containing more ions than the average transmit most of the tunnel current. As the dimensions of such areas may be smaller than the wavelength of the electron tunneling, diffraction may be significant, weakening the conservation of k parallel to the junction, and possibly broadening the minimum in dI/dV at $eV = \mu_F$.[14]

The conductance threshold at 18.3 mV in Fig. 7 is believed to represent the onset of the Kleinman[17,42] two-step tunneling process in which an electron of energy exceeding $\hbar\omega_{TA}$ first tunnels from the metal into a virtual state at $k = 0$ in the semiconductor, and then scatters from $k = 0$ to k_0 with emission of a TA phonon of wave vector $-k_0$. Proper phonon structure also occurs at $V = -18.3$ mV but is too weak to be evident in Fig. 7.

The majority of junctions were fabricated with Au electrodes because of the chemical inertness of the Au surface. Junctions fabricated with Ni and In showed slightly increased conductance per unit area, but were not different in other respects.[11] In the case of In, the proper superconducting density-of-states structure appeared in the tunneling spectrum at temperatures below the transition temperature of 3.41 °K.

B. Resonant Scattering Peak

A conductance peak of magnitude $\Delta G/G_0 \sim 10\%$ at 1.3 °K and width ~2 mV can be seen near $V = 0$ in Fig. 7, and is a characteristic feature of these vacuum-cleaved junctions. In Fig. 9(a) an enlarged view of dV/dI is shown. As previously reported,[11] $\Delta G/G_0$ is independent of the metal chosen as the electrode but depends systematically on the donor concentration N_D. In addition, we find that at fixed N_D the peak depends on the donor species. At 1.3 °K we find $\Delta G/G_0 \approx 7\%$ in Si: (1.6×10^{19} cm^{-3} P) and $\Delta G/G \approx 13\%$ in Si: (1.6×10^{19} cm^{-3} As), while in other respects the spectra are similar. This increase correlates with increased binding energy of the As donor, 53 meV as compared to 45 meV for P.

In order to study the scattering peak in detail, it is essential to separate carefully the anomalous conductance from the background. There is every indication, theoretically[6] and experimentally, that the anomalous conductance is symmetric about $V = 0$. The conductance peak appears on a background that decreases approximately linearly with bias V, and hence has a substantial component odd in V. For these reasons the even conductance

$$G^{(E)}(V) \equiv \tfrac{1}{2}[G(+V) + G(-V)] \qquad (4.1)$$

was computed, after converting the dV/dI data to $G(V) = (dV/dI)^{-1}$. We emphasize that this is permissible because the $G^{(2)}$ and $G^{(3)}$ conductances are even in voltage,[6] and very useful because the background $G(V)$, apart from a constant, is nearly an odd function of V. The remaining even component

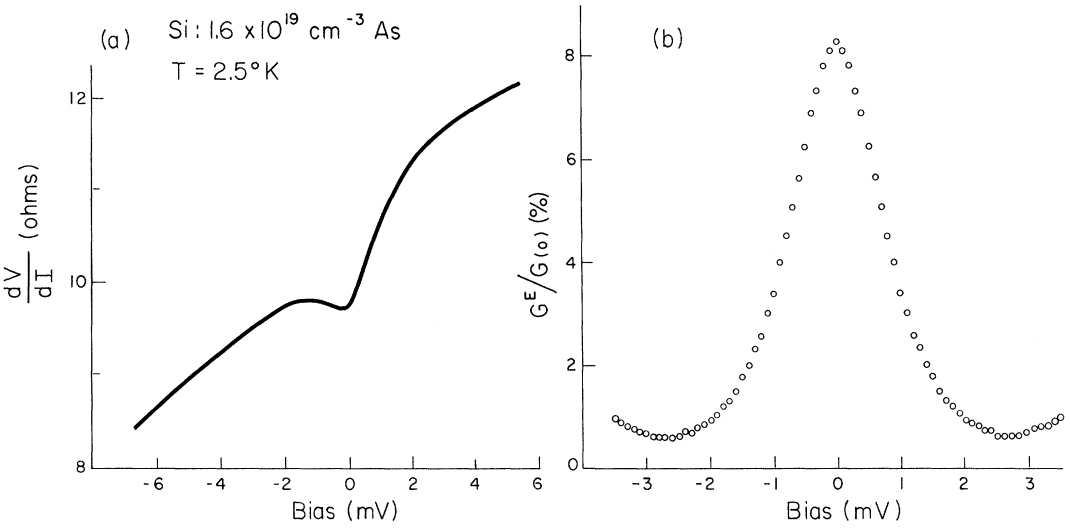

FIG. 9. (a) Detail of dV/dI spectrum near $V=0$, for Au | Si:As junction, showing zero-bias anomaly. (b) Even component of the conductance $G^{(E)}(V)$ obtained from curve in Fig. 9(a). Approximately parabolic residual background conductance is evident beyond 3-mV bias. Theory predicts $G^{(2)}(V)$ and $G^{(3)}(V)$ to be even functions of bias voltage V.

of the background amounts typically to $\lesssim 10\%$ of $G^{(3)}(0)$, and is well approximated by a parabola βV^2. Figure 9(b) shows the $G^{(E)}(V)$ corresponding to Fig. 9(a) and illustrates the typical even background. A computer program found $G^{(E)}(V)$ and fitted the best parabolic background to $G^{(E)}(V)$ in the voltage range 3.0–3.5 mV. This background conductance was then subtracted to obtain $G^{(3)}(V)$. These steps were carried out on each of a set of dV/dI curves representing a set of temperatures. Resulting $G^{(3)}(V)$ spectra are shown in Fig. 10 for several temperatures. The sharpening of the anomalous scattering peak with decreasing temperature is a striking feature of these curves. An important test of the anomalous scattering is a plot of the magnitude $G^{(3)}(0)/G_0$ of the zero-bias conductance peak versus $\log T$. As shown in Fig. 11(a), for one As and two P junctions there are no significant deviations from the straight-line $\log T$ dependence for temperatures between 4.2 and 1.3 °K. In the case of one additional As junction, shown in Fig. 11(b), measurements extended from 3.6 to 0.36 °K, again consistent with the $\log T$ dependence. The intercepts at $G^{(3)}(0)/G_0 = 0$ range from 7 to 11 °K and are somewhat higher for P as compared to As junctions.

We next compare the energy dependence $G^{(3)}(V)$ with the Kondo-Appelbaum integral function $F(eV)$, Eq. (2.29). This was accomplished by fitting the corresponding interpolation function,

$$G^{(3)}(V) = -A \ln\{[(eV)^2 + W^2]/E_0^2\}^{1/2}, \qquad (4.2)$$

to each $G^{(3)}(V)$ curve. The best values in the sense of least squares of A, W, and E_0 were obtained by computer. This routine was carried out on curves representing several temperatures on five different junctions.

A set of comparisons typical of many obtained is shown in Fig. 12. The fits are excellent at 4.2 °K, while small systematic deviations are noticeable below 2 °K in all junctions studied. One should bear in mind that these deviations must leave undisturbed the $-\log T$ dependence of $G^{(3)}(0)$.

In Fig. 12(f) the interpolation function is fitted to numerically computed values of the integral function $F(eV)$. The fitted values of the parameter W, which, according to numerical studies of the Kondo integral, should increase nearly linearly with temperature, are plotted T in Fig. 13.

The values of W for several junctions, representing both As and P donors, lie close to a line $W = \alpha k_B T$, with $\alpha = 2.12$. The fitted values of E_0 are near 2 meV, with a tendency to decrease slightly at lower temperatures, for both P and As junctions. Since A and E_0 are approximately independent of temperature, the function (4.2), with $W = 2.12 k_B T$, quite well describes the spectra on a given junction over a set of temperatures. The accuracy of this approximation is indicated in a "universal" plot, Fig. 14, of $G^{(3)}(V)$ values measured at 0.1-mV intervals on a Si:As junction at seven temperatures, versus $\ln[(eV)^2 + (2.12 k_B T)^2]^{1/2}$.

C. Effect of High Magnetic Fields

Figure 15 shows dV/dI traces near $V=0$ from a Si:As junction, $T = 1.3$ °K, at magnetic fields ranging up to 150 kOe. Plots of the even conductance,

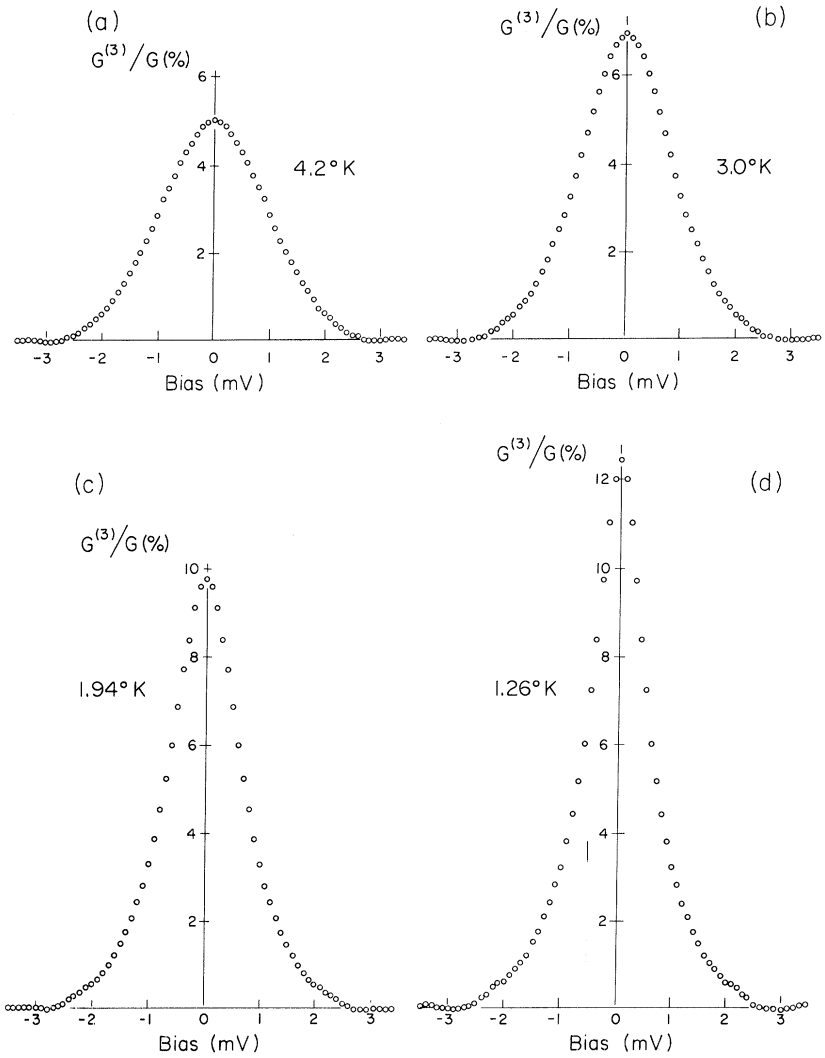

FIG. 10. Anamalous conductance $G^{(3)}(V)$ for a Au | Si : As junction at several temperatures. Curves *a*, *b*, *c*, and *d* correspond to $T = 4.2$, 3.0, 1.94, and 1.26 °K, respectively.

Eq. (4.1), after subtraction of the background, corresponding to $G^{(3)}(V, H) + G^{(2)}(V, H) - G^{(2)}(V, 0)$, are shown in Fig. 16, for two temperatures. Important features of the behavior are:

(a) The conductance peak disappears at high field and is replaced by a conductance dip which increases in magnitude (up to ~ 10%) and half-width (up to ~ 1 mV) with magnetic field.

(b) The field-induced dip is severely broadened, and the broadening also increases with field.

(c) The background conductance $|V| \geq 3$ mV is unaffected by the magnetic field. This implies that the basic barrier parameters are essentially unchanged by the field. Condition (c) indicates further that the number of moments is independent of field.

We may estimate, in order of magnitude, the number of localized donor magnetic moments needed to produce the observed 10% conductance dip at $|eV| < g\mu_B H$ from the spin-exchange cross section $\sigma_x = 2\times10^{-12}$ cm^2, discussed in Sec. IID. It follows from Eq. (2.24) for the spin-flip conductance $G^{(2)}$ that the maximum field-induced fractional change $\Delta G^{(2)}/G^{(2)}$ is $S/(S+1)$, or $\frac{2}{3}$ for $S = \frac{1}{2}$. Thus we can estimate $G^{(2)}/G_0 \approx 0.15$. Assuming a thin layer of magnetic moments of surface density N_a (cm^{-2}), the probability of an electron undergoing a spin flip in traversing this layer is very roughly $G^{(2)}/G_0$. If the cross section for the process is σ_x, then $N_a\sigma_x \sim G^{(2)}/G_0$, which gives $N_a \sim 10^{11}$ cm^{-2}. This compares favorably with the previous estimate, Eq. (2.57), of $N_a = 0.6\times10^{11}$ cm^{-2} based on the model of a local Mott transition in the reserve region. Note that the implied spacing between moments is large, approximately 150 Å.

The nature of the high-field conductance dip is more clearly revealed in second derivative. Direct tracings of several d^2V/dI^2 curves are shown in Fig. 17. Typical reduced d^2I/dV^2 spectra for

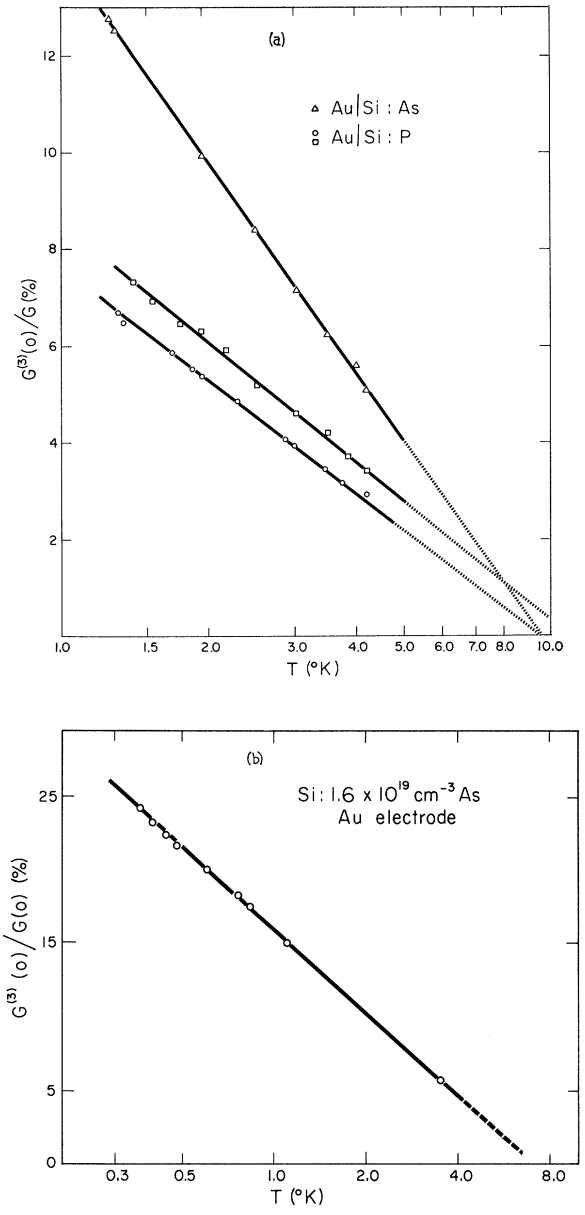

FIG. 11. (a) Plots of the Kondo peak $G^{(3)}(0)$ versus $\log T$ for one Au | Si:As and two Au |Si:P junctions. Conductance background has been subtracted, as discussed in the text. Increase of $G^{(3)}(0)$ in Si:As as compared to Si:P correlates with the larger binding energy of the As donor. (b) Plot of the Kondo peak $G^{(3)}(0)$ versus $\log T$ for a single Au | Si:As junction extending to a lowest temperature of 0.36 °K. Note the 25% magnitude of $G^{(3)}(0)$ at 0.36 °K and that the points do not deviate significantly from a straight line.

Au|Si:As are shown in Fig. 18(a). Since $d^2I/dV^2 = (d/dV)G(V)$ is the derivative of a function even in voltage, and hence an odd function, we have plotted the odd part of d^2I/dV^2. No attempt was made to subtract the background. The curves in Fig. 18(a) reveal that at high field, d^2I/dV^2 consists approximately of a broad peak at $eV = \Delta$, which we identify as the spin-flip threshold. For the moment, as an approximation we ignore possible $dG^{(3)}/dV$ contributions at high field and proceed to plot in Fig. 19 the peak position Δ and half-width Γ, defined in Fig. 18(a), against H. Since the Zeeman transition apparently overlaps zero energy, we have estimated Γ from the high-energy half of the peak. The values of Δ plotted in Fig. 19 fall reasonably on a straight line through the origin, in support of our approximate analysis. The slope of Δ versus H determines a g value, which is 1.18 ± 0.04 for the As donor, corresponding to a large negative g shift $\Delta g = -0.82$ on the assumption $g_0 = 2.0$. In the case of P donors, the g value is similarly found to be 0.98 ± 0.04.

The second important feature in Fig. 19 is the large value and proportionality to H of the half-width $\Gamma = 0.65\Delta$ for As donors. We identify this half-width with the lifetime-broadening equation (2.35), from which, with the experimental g shift and Eq. (2.33), we obtain a theoretical width $\Gamma_t = 0.53\Delta$. Similar agreement is obtained in the case of P donors, where $g = 0.98$ and $\Gamma = 0.84\Delta$ compares favorably with $\Gamma_t = 0.81\Delta$. A consistent understanding of the small g value and large width Γ is thus achieved as a direct consequence, through Eqs. (2.33) and (2.35), of the exchange-interaction equation (1.1). These results are approximate and depend on justification of the assumption that at high fields the $dG^{(3)}/dV$ contribution is small.

We have verified that this is the case by calculating the $(d/dV)G^{(3)}(V, H)$ implied by the theory at high field, given the experimental values of g, Γ, and the zero-field spectrum $(d/dV)G^{(3)}(V, 0)$. We find that properly including the intrinsic high-field broadening Γ via Eqs. (2.38) and (2.39) in the Kondo integral (2.29) over intermediate spin-flipped states in the third-order process greatly reduces $dG^{(3)}/dV$ at high field. This is shown in Fig. 20, where for 150 kOe and $T = 1.25$ °K, a comparison is made between $dG^{(3)}/dV$ calculated with $\Gamma = 0.65$ meV and with $\Gamma = 0$. The cutoff E_0 has been set at 6 meV, somewhat greater than the fitted value, to avoid artificial effects at eV, $\Delta \approx E_0$. For voltages $eV \ll E_0$, the calculated curves are insensitive to E_0. Similarly calculated $dG^{(2)}/dV$ curves are shown in Fig. 21. Comparison of theory with experiment is shown in Fig. 18(b), where the $dG^{(3)}/dV$ is calculated using $\Gamma = 0.65$ meV, $g = 1.18$, and normalized by comparison to the $H = 0$ experimental curve, Fig. 18(a). The upper dashed curve is $dG^{(2)}/dV$, also corresponding to $\Gamma = 0.65$ meV and $g = 1.18$, with normalization adjusted by comparison of the summed contributions (the upper solid curve) with the experimental curve i in Fig. 18(a). The required ratio of $dG^{(3)}/dV$ to $dG^{(2)}/dV$ is signifi-

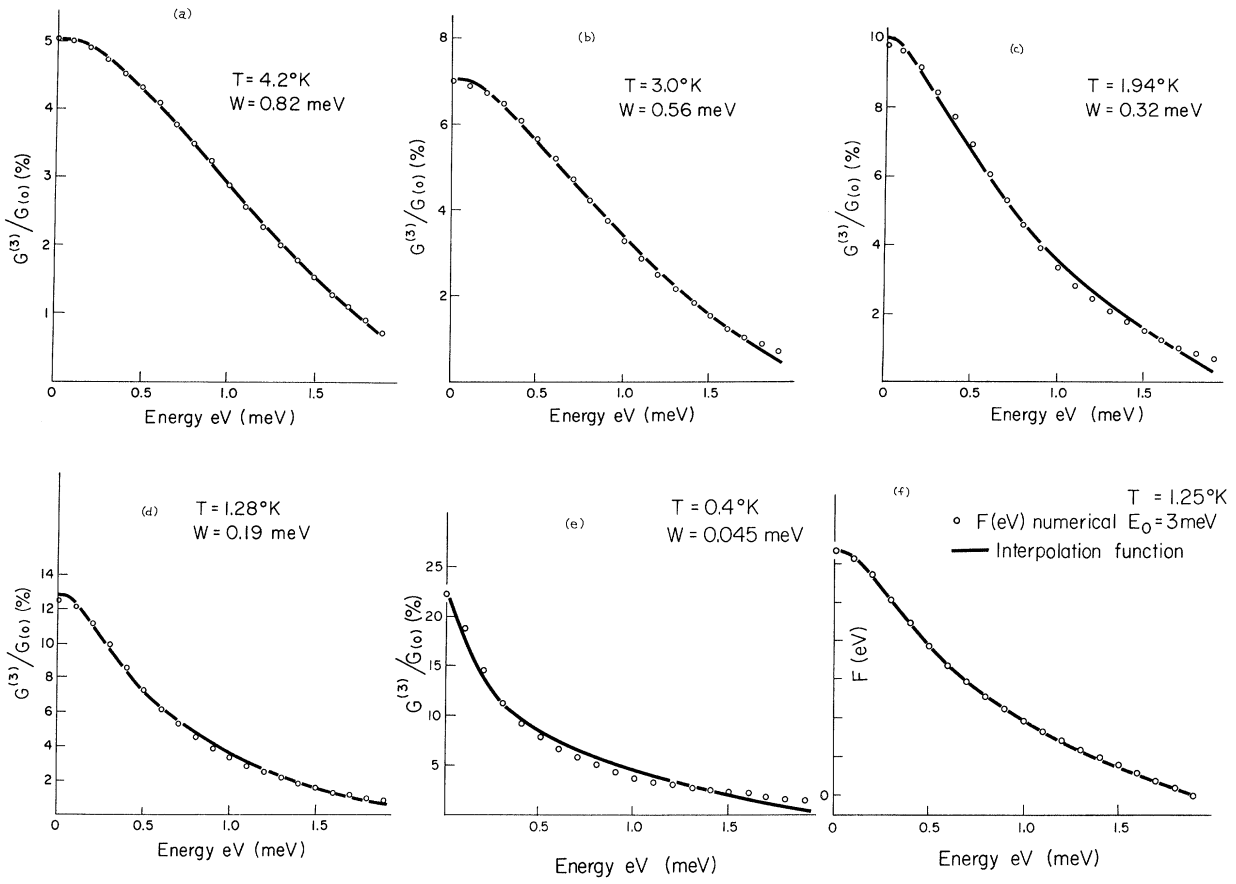

FIG. 12. (a)–(e) Energy dependence $G^{(3)}(eV)$ of the Kondo conductance, shown as circles, compared with the interpolation function, Eq. (4.2), for a Au | Si : As junction at temperatures 4.2, 3.0, 1.94, 1.28, and 0.4 °K. (f) Comparison of the interpolation function (4.2) with numerically computed values, shown as circles, of the Kondo integral, Eq. (2.29). Values $E_0 = 3$ meV and $T = 1.25$ °K were taken in computing the integral.

cantly less than predicted by theory.[6] We will return to this point below. Figures 22 and 23 display $G^{(3)}(V, H)$ and $G^{(2)}(V, H) - G^{(2)}(V, 0)$ similarly calculated. Note in Fig. 22 the degree to which the high-field conductance "overshoot" is reduced by properly including the broadening effect. Finally, in Figs. 24(a) and 24(b) we show families of theory curves, $G(V, H)$ and $(d/dV)G(V, H)$, respectively, which are to be compared with the experimental curves in Figs. 16 and 18(a). The ratio of $G^{(2)}$ to $G^{(3)}$ in Figs. 24(a) and 24(b) is that determined in Fig. 18. We emphasize that all theoretical curves, except those labeled $\Gamma = 0$, have been calculated from Eqs. (2.24), (2.28), and (2.29), in which the broadening Γ is included by averaging all $\tanh(\frac{1}{2}\beta\epsilon)$ and $H(\beta\epsilon)$ functions over a Lorentzian distribution of width Γ, via Eqs. (2.38), (2.39), and (2.42). The same convolution has been applied to the $\tanh(\frac{1}{2}\beta\epsilon)$ representing the magnetization $\langle M\rangle$ for $S = \frac{1}{2}$, to treat approximately the large broadening Γ which accompanies the splitting Δ. Thus we have taken $\langle M\rangle = S(\Delta)$, Eq. (2.38). Note that this procedure would be strictly correct in the case of an *inhomogeneous* width Γ.

As we have noted in Sec. II, the scattering occurring at $V = 0$ is the direct analog of scattering in bulk samples containing magnetic moments. Thus measurement of the conductance change ΔG at $V = 0$ is equivalent to a magnetoresistance measurement. The results for a Si : As junction at 1.25 °K are shown in Fig. 25. It can be argued[6] that in the low-field limit, scattering from a magnetic system should be proportional to $\langle M\rangle^2$. If $\langle M\rangle \propto H$, then the conductance change will be proportional to H^2. Although this low-field behavior is not shown in Fig. 25, we have in fact verified the H^2 dependence for fields between 2 and 8 kOe. Further, we find, for all fields, that $\Delta G(0, H)$ is nearly a function of H/T as expected. These considerations should hold even in the presence of third-order scattering.

Included in Fig. 25 as the conductance change $\Delta G^{(2)}$ and $\Delta G^{(3)}$ calculated on the basis of the con-

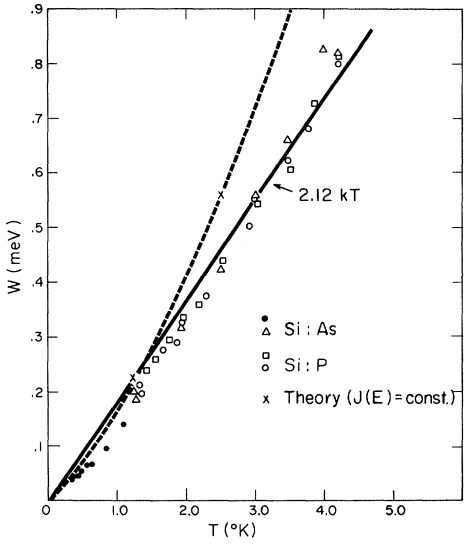

FIG. 13. Fitted values of the parameter W in Eq. (4.2) plotted against the temperature T, for several junctions. Each point in this plot corresponds to a fitted $G^{(3)}$ spectrum, such as those shown in Fig. 12. Dashed line is the variation of W with T indicated by numerical studies of the Kondo integral, Eq. (2.29).

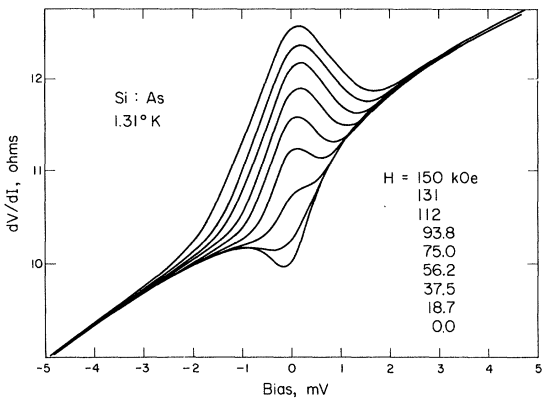

FIG. 15. Effect of magnetic field on the dV/dI spectrum near $V=0$, for a Au | Si : As junction at 1.25 °K. Magnetic field is perpendicular to current flow. Magnetic fields increase to 150 kOe, as labeled. Note independence of baseline of magnetic field.

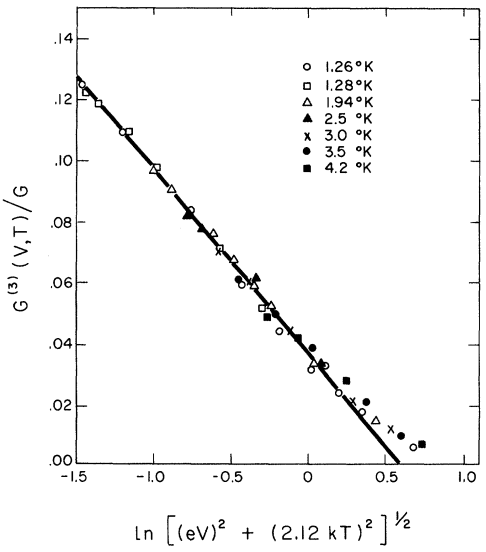

FIG. 14. Comparison of measured spectra at 0.1-mV intervals on a Au | Si : As junction at seven temperatures with the interpolation function Eq. (4.2). Value $W = 2.12 k_B T$ corresponding to the solid line in Fig. 13 has been assumed.

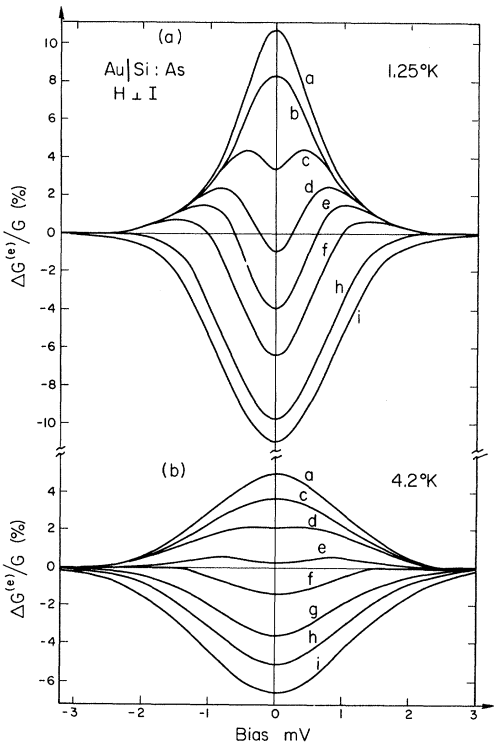

FIG. 16. Effect of magnetic field on the conductance peak at (a) 1.25 and (b) 4.2 °K. Curves labeled a, b, c, d, e, f, g, h, and i correspond to magnetic fields 0, 18.8, 37.5, 56.3, 75.0, 93.8, 112.5, 131.2, and 150 kOe, respectively. These results for $\vec{H} \perp \vec{I}$ are similar to results with $\vec{H} \parallel \vec{I}$.

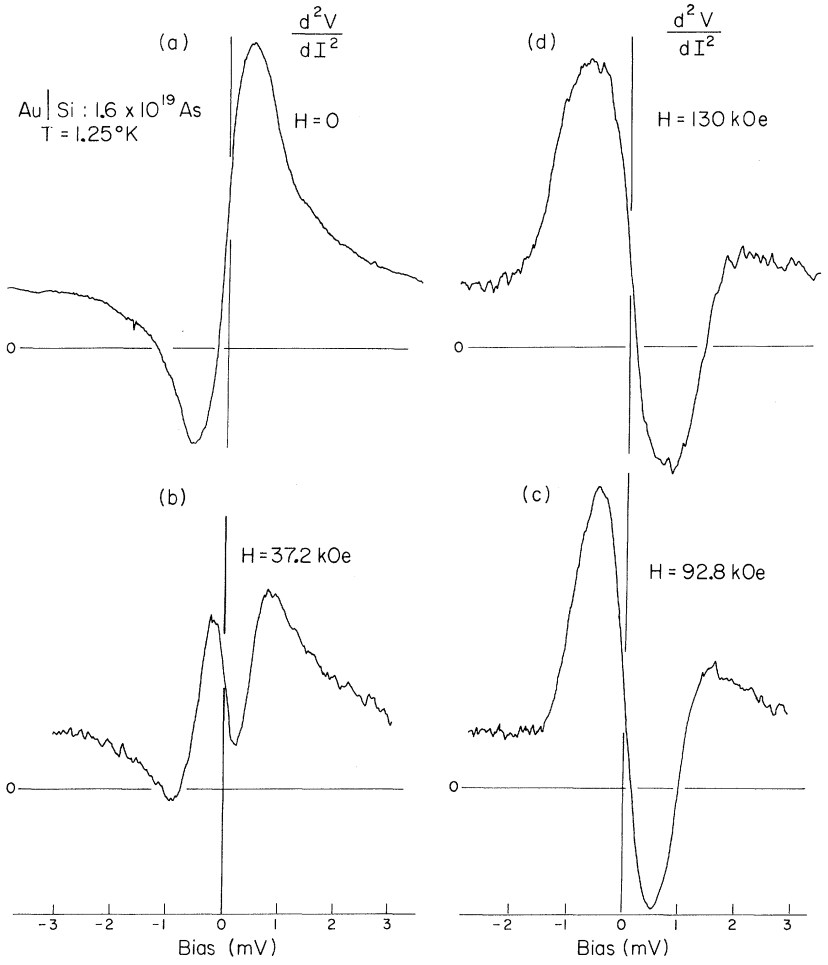

FIG. 17. Direct tracings of d^2V/dI^2 curves at fields 0, 37.2, 92.8, and 130 kOe in (a), (b), (c), and (d), respectively.

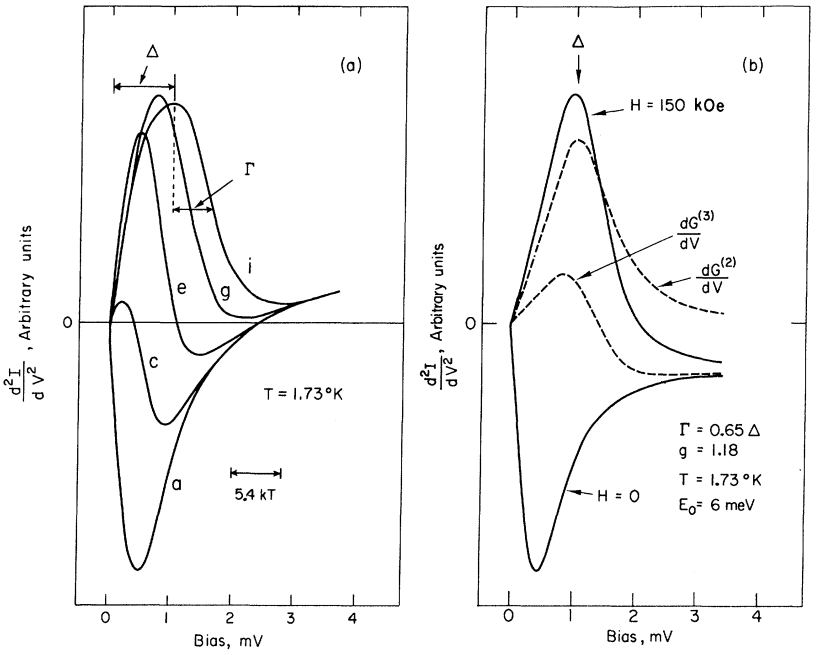

FIG. 18(a). Effect of magnetic field on d^2I/dV^2 for Au | Si : As junction at 1.73 °K. Odd part of d^2I/dV^2 is plotted. Curves *a*, *c*, *e*, *g*, and *i* correspond to 0, 37.5, 75, 112.5, and 150 kOe, respectively. High-field d^2I/dV^2 peak closely approximates the Zeeman transition spectrum of the local moments. (b) Theoretical d^2I/dV^2 curves calculated for $H=0$ and $H=150$ kOe for parameter values indicated. Ratio $G^{(3)}/G^{(2)}$ has been adjusted to match curves *a* and *i* in Fig. 18(a), as described in text.

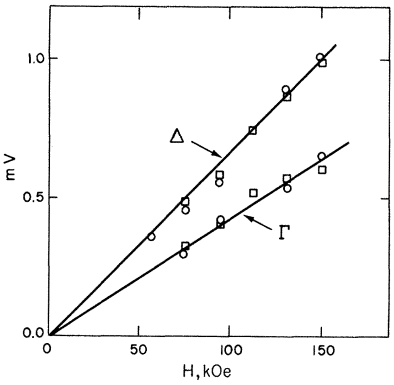

FIG. 19. Plots of estimated Zeeman splitting Δ and half-width Γ versus H for Au | Si : As junction. Γ and Δ are defined in Fig. 18 (a). Circles, 1.25 °K; squares, 1.73 °K.

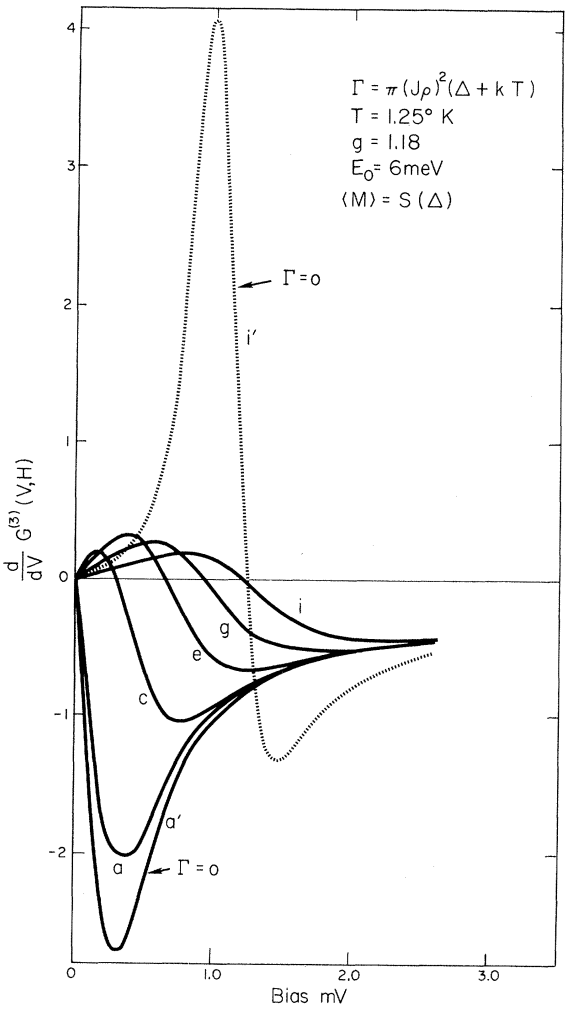

FIG. 20. Calculated $dG^{(3)}/dV$ curves for fields 0, 37.5, 75, 112.5, and 150 kOe are labeled a, c, e, g, and i, respectively. Small zero-field Korringa broadening is included here and below by taking $\Gamma = \pi(J\rho_F)^2(\Delta + k_B T)$. In curves a' and i', the broadening Γ is set to zero, for $H = 0$ and $H = 150$ kOe. Comparison of curves i and i' reveals magnetic field quenching of the Kondo scattering.

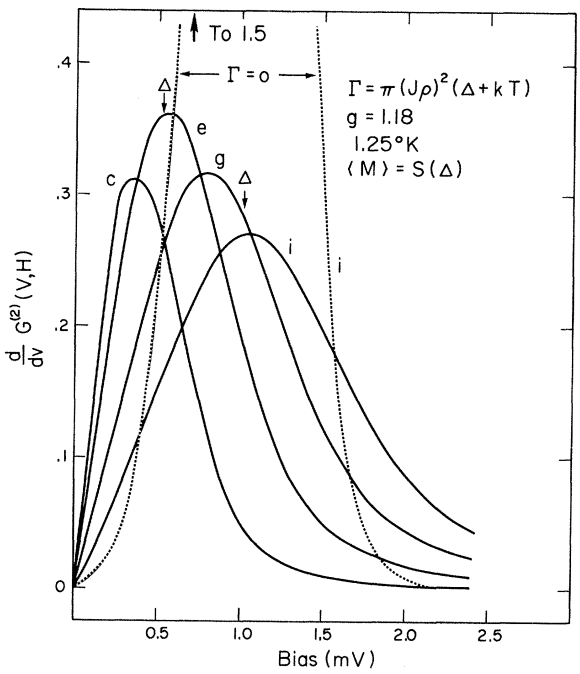

FIG. 21. Calculated $dG^{(2)}/dV$ curves for fields 37.5, 75, 112.5, and 150 kOe are labeled c, e, g, and i, respectively. In curve i' the broadening Γ is set to zero, for $H = 150$ kOe.

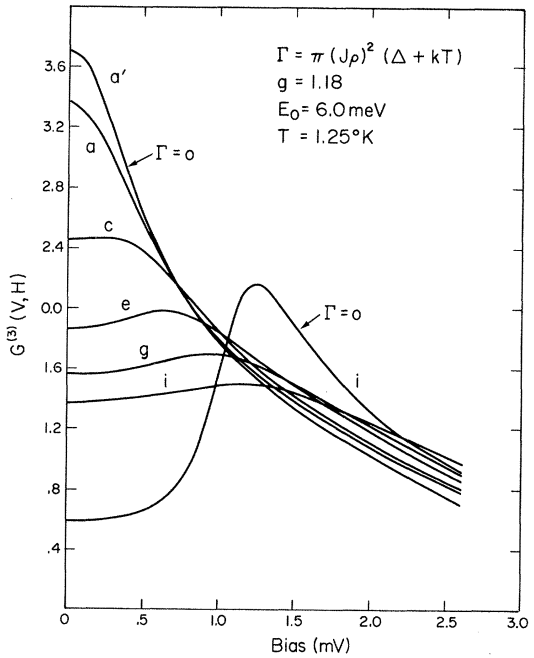

FIG. 22. Calculated $G^{(3)}(V,H)$ curves for fields 0, 37.5, 75, 112.5, and 150 kOe are labeled a, c, e, g, and i, respectively. Curves a' and i' have been calculated neglecting the broadening Γ. "Overshoot" of $G^{(3)}(V)$ at high field is greatly reduced by proper inclusion of broadening Γ.

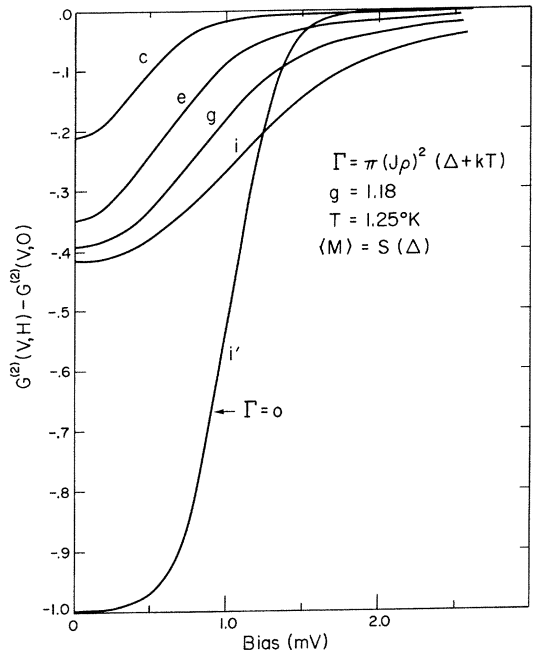

FIG. 23. Calculated $G^{(2)}(V,H) - G^{(2)}(V,0)$ curves for fields 37.5, 75, 112.5, and 150 kOe are labeled *c*, *e*, *g*, and *i*, respectively. Curve *i* is shallower than curve *i'*, calculated for 150 kOe with $\Gamma = 0$, in part by the choice $\langle M \rangle = S(\Delta)$, as explained in text.

siderations of Sec. II. As explained above, the average magnetization $\langle M \rangle$ has been taken to be $S(\Delta)$ rather than the usual Brillouin function $\tanh(\frac{1}{2}\beta\Delta)$, to treat approximately the large broadening Γ accompanying the splitting Δ. The calculated values of $\Delta G^{(2)}(0)$ (the dashed line) and $\Delta G^{(3)}(0)$ (the squares) saturate less rapidly with increasing field would be the case for $\Gamma = 0$, i.e., for $\langle M \rangle = \tanh(\frac{1}{2}\beta\Delta)$. On the other hand, the calculated values saturate more rapidly than the experimental curve (circles). We believe that the absence of good agreement here reflects our lack of firm knowledge of $\langle M \rangle$ as a function of H in the presence of strong exchange coupling. The properties of the exchange-coupled magnetic moments revealed by the tunneling measurements are compiled in Table I. Additional parameters may be derived from the information in the table. The Anderson level width Γ_A from Eq. (2.54), having taken $U \approx 2E_0$, is estimated to be ~0.65 meV for As and ~0.80 meV for P. The values of E_0 and $J\rho_F$ and Eq. (1.2) predict T_K values of 2.0 and 3.2 °K for As and P, respectively. The theory [Eq. (5.1) below] also allows a prediction of the ratio $G^{(3)}(0)/\Delta G^{(2)}_{max}$. We discuss these inferences in detail in the following section.

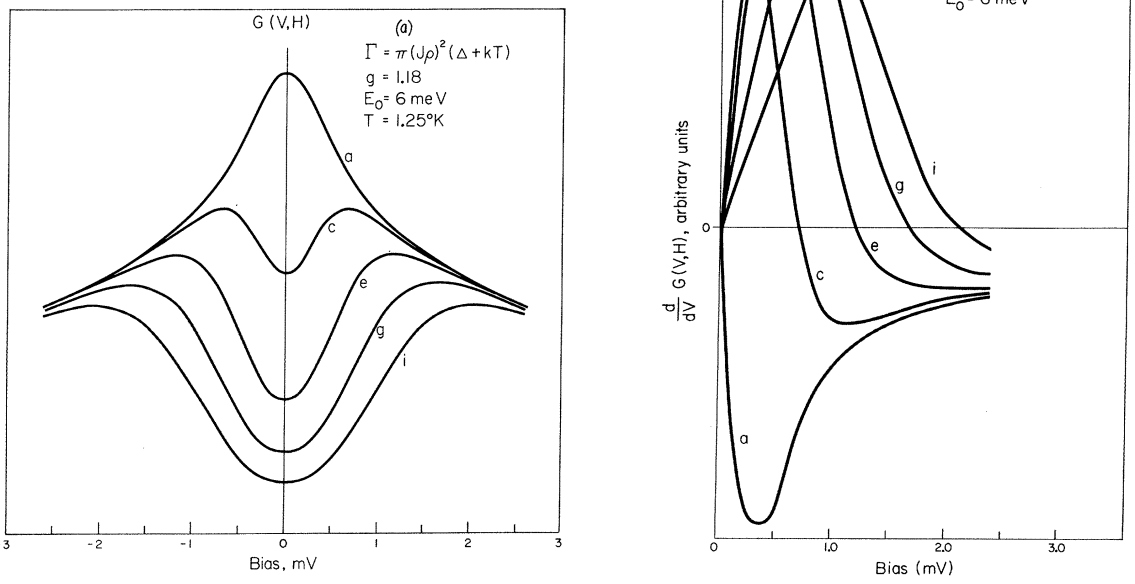

FIG. 24. (a) Calculated $G(V,H)$ spectrum to be compared with experimental curves in Fig. 16(a). Curves labeled *a*, *c*, *e*, *g*, and *i* correspond to 0, 37.5, 75, 112.5, and 150 kOe, respectively. Ratio of $G^{(2)}/G^{(3)}$ is consistent with Fig. 24(b). (b) Calculated $(d/dV)G(V,H)$ spectra to be compared with Fig. 18(a). Ratio $G^{(2)}/G^{(3)}$ has been adjusted to fit curves *a* and *i* of Fig. 18(a).

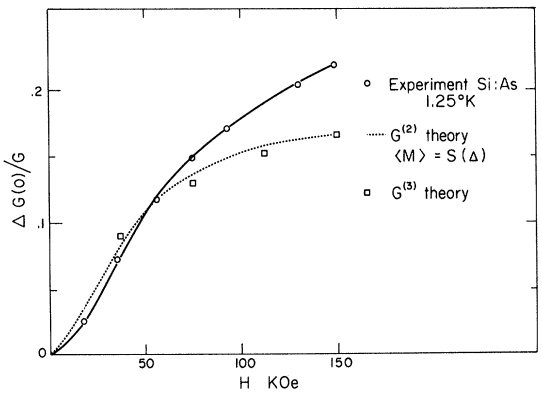

FIG. 25. Magnetic-field-induced reduction in conductance at $V=0$ versus magnetic field. Circles, data for Au | Si:As at 1.25 °K; dotted line, theory for $G^{(2)}$, computed with $\langle M\rangle = S(\Delta)$; squares, computed from $G^{(3)}$ theory.

V. DISCUSSION OF EXPERIMENTAL RESULTS

The zero-field spectra representing the energy dependence of Kondo scattering across the tunnel barrier shown in Fig. 12 are in good agreement with the Appelbaum-Kondo perturbation theory. The temperature dependence $G^{(3)}(0) \propto -\log T$ was accurately verified down to 1.25 °K on many junctions [Fig. 11(a)] and down to 0.36 °K in one case, shown in Fig. 11(b). We have never observed a deviation from this behavior. Note that this conclusion follows directly from the data by subtraction of the background, in which we have been particularly careful, and does *not* involve assumptions about the functional form of $G^{(3)}(eV)$.

One can infer from this, first, that both the Zeeman levels of the local moment at $H=0$ *and the semiconductor final states* at the Fermi energy are sharply defined on an energy scale of $k_B T$, or about 3×10^{-5} eV at 0.36 °K. These level widths both appear in the denominator of the integral in Eq. (2.37) and must cut off the $\log T$ dependence[21] at $\log(\Gamma/k_B)$. Thus, interaction between the local moments, e.g., the Ruderman-Kittel coupling considered by Suhl,[21] does not measurably broaden the Zeeman levels.[43] The extreme sharpness, ≈ 0.03 meV, implied for the semiconductor final states is evidence that they are representative of the bulk of the electrode rather than of some surface layer. From the uncertainty principle, the electron must remain in the final state for an interval $\Delta t \geq \hbar/\Delta E$, since its energy has been measured with an error not exceeding ΔE. For $\Delta E = 3\times10^{-5}$ eV, this implies $\Delta t \geq 2\times10^{-11}$ sec. But the final state is characterized by the Fermi velocity $v_F \cong 1.5\times10^{7}$ cm/sec, and a mean free path $l \geq 50$ Å. Hence, during the measurement, the electron traverses a depth at least $\Delta z \simeq \sqrt{(v_F l \Delta t)} \approx 1000$ Å. Since this greatly exceeds the dimensions $z_0 = 84$ Å and $\lambda \approx 10$ Å characterizing the interface, we are justified in associating the final states with the Fermi surface in the bulk of the electrode. This conclusion, which probably is also valid in other instances of tunnel junctions on cleavage planes of degenerate semiconductor, shows that it is quite possible to probe bulk properties in such experiments.

Second, observation of the accurate $-\log T$ dependence as predicted by the perturbation treatment indicates that complications related to the low-temperature divergence and possible quasibound state are not dominant in the temperature range of the experiment. This supports analysis of the magnetic field effects by extending the perturbation theory of Kondo and Appelbaum, but raises questions about the prediction, via Eq. (1.2), of T_K values of 2 and 3 °K.

Minor departures occur at low temperatures from the energy dependence of $G^{(3)}(V)$ predicted by the integral $F(eV)$, Eq. (2.29). We believe that these departures do not imply a failure of perturbation

TABLE I. Properties of magnetic moments in Schottky-barrier tunnel junctions on Si with donor concentration $1.6\times10^{19}\,\mathrm{cm}^{-3}$. E_D is the isolated donor binding energy; $G^{(3)}/G_0$ is the relative magnitude of the anomalous (Kondo) conductance; g is the g value of the local moment; $J\rho_F$ is the exchange-coupling parameter; Γ_{calc} is computed from Eq. (2.35); and Γ_{obs} is the experimentally observed linewidth. E_0 is obtained from fit of Eq. (4.2) to the zero-field spectra. Values of $G^{(3)}(0)/\Delta G^{(2)}_{\mathrm{max}}$, where $G^{(2)}_{\mathrm{max}}$ is the maximum field-induced conductance dip, are taken from curves such as those shown in Fig. 16. Other parameter values applicable in both cases are $S=\frac{1}{2}$, $g_0=2$, $N_A \sim 10^{11}\,\mathrm{cm}^{-2}$, $a_0^* \approx 20$ Å, $\sigma_x = 2\times10^{-12}\,\mathrm{cm}^2$, $z_0 = 84$ Å, and $\mu_F = 21$ meV. Assuming $\rho_F = 3N_D/4\mu_F$, estimates of J are 11 and 14 meV for P and As donors, respectively.

Donor species	E_D (meV)	$\left.\frac{G^{(3)}}{G_0}\right\|_{1.25\,°K}$	g	$J\rho_F = \frac{\Delta g}{g_0}$	$\frac{\Gamma_{\mathrm{calc}}}{g\mu_B H}$	$\frac{\Gamma_{\mathrm{obs}}}{g\mu_B H}$	E_0 (meV)	$\left.\frac{G^{(3)}(0)}{\Delta G^2_{\mathrm{max}}}\right\|_{1.25°K}$
As	53	~0.12	1.18 ±0.04	−0.41 ±0.02	0.53 ±0.05	0.65 ±0.03	2.0±0.2	0.6±0.1
P	45	~0.07	0.98 ±0.04	−0.51 ±0.02	0.81 ±0.08	0.84 ±0.04	2.1±0.2	0.75±0.1

theory; such a failure would imply also an important deviation[2-5] of $G^{(3)}(0)$ from $-\log T$, which does not occur. A more likely explanation is an energy dependence in the exchange J, perhaps that predicted by the Anderson model,[19] which is neglected, apart from introducing the cutoff E_0, in the theory. That energy dependence in J may be more important here than is metal-insulator-metal junctions is suggested by the small fitted values of E_0[13,44] near 2 meV.

While the energy and temperature dependence of $G^{(3)}(V)$ are in good agreement with the theory, we find that Appelbaum's theory,[6] using the fitted values of E_0 and $J\rho_F$, overestimates the magnitude of Kondo scattering $G^{(3)}(V)$ relative to spin-flip scattering $G^{(2)}(V)$. The magnitude of Kondo scattering at zero bias, $G^{(3)}(0)$, compared with the maximum field-induced change in spin-flip scattering

$$\Delta G^{(2)}_{\max} = \lim_{H\to\infty}[G^{(2)}(0,0) - G^{(2)}(0,H)],$$

from Eqs. (2.24), (2.28), and (2.29), is predicted to be

$$G^{(3)}(0)/\Delta G^{(2)}_{\max} = 8S(S+1)J\rho_F^2 \ln(E_0/\alpha k_B T). \quad (5.1)$$

For the case of an As-doped junction at 1.25 °K as shown in Table I, the directly measured ratio $G^{(3)}(0)/\Delta G^{(2)}_{\max}$ is ≈ 0.6. This is considerably smaller than the theoretical value, using $S=\frac{1}{2}$, $-J\rho_F = 0.41$, $E_0 = 2$ meV, and $\alpha = 2.1$, which from Eq. (5.1) is 5.3. This discrepancy with the theory[6] suggests that the effective expansion parameter in the perturbation series is not $J\rho_F \ln(E_0\alpha k_B T)$ but a smaller number. This could also explain why no deviations from the $\log T$ dependence related to slow convergence in the series are seen, and thus could make Eq. (1.2) an overestimate of the divergence temperature. The directly measured values of $J\rho_F$ and E_0 and Eq. (1.2) determine a temperature $T_K = (E_0/k_B)\, e^{1/J\rho_F}$ at which deviations from the perturbation results should be important. The perturbation series is actually infinite at $0.77T_K$.[4] The prediction of T_K for Si:As is 2 °K, considerably above the lowest temperature reached, 0.36 °K. We will limit our discussion to the As case, since the data cover a wider temperature range than in the case of P.

Since the prediction of T_K from Eq. (1.2) is quite sensitive to the value of $J\rho_F$ it is worthwhile first to discuss possible sources of error. The expected error in $-J\rho_F$ from experimental error in the g-value measurement is about 5%. There may be some systematic error in obtaining E_0 for Eq. (1.2) from the interpolation function, Eq. (4.2), but not enough to remove the discrepancy.

A possibility for an overestimate of $-J\rho_F$ from the observed g shift is that the true susceptibility of the conduction-electron spin system is not accurately described by the Pauli formula, Eq. (2.32), but is enhanced by a factor $(1+\beta)$, $\beta > 0$. Thus $\chi = \chi_P(1+\beta)$. It is conceivable, since the degenerate semiconductor has a donor concentration only about four times the Mott critical concentration, that an exchange enhancement[45] could be as large as 30%. In this case $\frac{1}{2}(g-g_0) = J_{\text{obs}}\rho_F = J(1+\beta)\rho_F$; an enhanced g shift would occur not because the exchange interaction is stronger, but because the conduction electrons would polarize more readily. A value $\beta \approx 0.3$ would lower the estimate of T_K by a factor of ~ 2, by reducing the estimate of $J\rho_F$. On the other hand, $\beta > 0$ will not increase the level broadening $\Gamma = \pi(J\rho_F)^2(g\mu_B H)$, so that on this interpretation the calculated value Γ_t would have to be multiplied by $(1+\beta)^{-2}$; thus a 40% reduction if $\beta = 0.3$. In view of the agreement between the observed Γ and the theoretical value Γ_t, it seems unlikely that β could be as large as 0.3.

We conclude, assuming the validity of Eq. (1.2) for T_K, that the experimental values imply $T_K = (2 \pm 1)$ °K for As donors. On the other hand, if T_K were as great as 1 °K, deviations from the $\log T$ dependence would be evident. We conclude that the true value of T_K must be below 1 °K, probably below 0.3 °K, and that Eq. (1.2) is incorrect in the present context.

It has been shown[46,48] that the effect of simultaneous potential scattering on exchange scattering is to reduce the coefficient of the logarithmic term $G^{(3)}(V)$ by a factor $f(\eta) = \cos^6\eta \cos 2\eta$. This lowers the divergence temperature, which is now determined by

$$T_K = (E_0/k_B)\, e^{(1/J\rho_F \cos^2\eta)} \quad J < 0. \quad (5.2)$$

Here η is determined by the strength of the potential scattering through the relation $\tan\eta = -\pi V\rho_F$. We assume that the simultaneous potential scattering does not change the relation $\Delta g = 2J\rho_F$. We can determine the value of η appropriate to As donor moments to restore agreement between theory and experiment for the ratio $G^{(3)}(0)/\Delta G^{(2)}{}_{\max}$, which becomes, for $S=\frac{1}{2}$,

$$G^{(3)}(0)/\Delta G^{(2)}{}_{\max} = 6J\rho_F \cos 2\eta \ln(E_0/\alpha k_B T). \quad (5.3)$$

Taking the experimental ratio 0.6 at 1.25 °K, we find $\cos 2\eta = 0.11$; thus $V\rho_F = -0.29$ and $\cos^2\eta = 0.55$. From Eq. (5.2), the resulting estimate is $T_K = 0.3$ °K for Si:As and, similarly, $T_K = 0.7$ °K for Si:P. These estimates are consistent with the observed $\log T$ dependence in Si:P to 1.3 °K and in Si:As to 0.36 °K. This satisfactorily resolves the discrepancy of $G^{(3)}/G^{(2)}$ with the Appelbaum theory and also explains the success of perturbation theory, i.e., the absence of strong-coupling deviations from $-\log T$ in the experimental results below 1 °K. We find the idea of potential scattering with $V\rho_F \approx -0.29$ to be plausible, particularly in view of the connection with the neutral donor, which, as de-

scribed in Sec. II D, is similar in its scattering properties to the hydrogen atom.[30] In this context some potential scattering would be expected.

The results discussed thus far depend on a microscopic model for the local moment primarily through the assumption $g_0 = 2$ made to determine $J\rho_F$ from the high-field spin-flip threshold.[49] The tunneling spectra with H and T as external parameters contain enough information to allow a fairly complete comparison with theory without a microscopic model for the moments. Indeed, some previous studies[13] have been carried out without such a model.

We have been interested, in addition, in understanding why local moments should occur in vacuum-cleaved Schottky-barrier junctions, and have proposed that they are transiently localized neutral donor states at the inner edge of the depletion region. As such they are well described by the Anderson model. The proximity of these states to the degenerate portion of the semiconductor and the close connection between the Anderson model[7] and the Hubbard model[34] are consistent with a strong electron-hopping interaction V_{kd} corresponding, through Eq. (2.51), to a large value of $\Gamma_A/U \gtrsim 0.1$. This in turn implies by Eq. (2.53) a strong antiferromagnetic s–d exchange coupling $-J\rho_F \gtrsim 0.25$. This picture is supported by the experiment, which gives for Si:As, $J\rho_F = -0.41$, or $\Gamma_A/U = 0.16$. A less precise relation $E_0 \approx \frac{1}{2}U$ gives $U \approx 4$ meV, and hence $\Gamma_A \approx 0.6$ meV, for the localized donor state.

A success of the model is agreement between the predicted local moment density $N_A \approx 0.6 \times 10^{11}$ cm^{-2}, obtained from an assumption of a local Mott transition, Eq. (2.57), and the estimate of N_a based on the donor spin-exchange cross section σ_x, and the observed magnitude of the spin-flip scattering conductance $G^{(2)}/G_0$. Finally, the increase in $G^{(3)}(0)$ and slight decrease in coupling strength $-J\rho_F$, in substituting As donors with a larger binding energy for P donors, is consistent with the model. One must consider, in addition, the previously noted donor concentration dependence,[11] the independence of the electrode metal, and the lack of an alternative explanation for magnetic moments in vacuum-cleaved junctions on substrates containing no transition-metal ions. In our view, the sum of this evidence is unequivocal support for the localized donor model. Indeed, it seems clear that the same model accounts for weak zero-bias conductance peaks that we have observed in CdS Schottky barriers,[50] those reported in GaAs,[51] as well as similar peaks which were described as early as 1962 as a fundamental feature of both Si and Ge p–n junctions.[52] As mentioned in Sec. II D, at dopant concentrations N, many times greater than the Mott concentration N_c, the localized donor magnetic moments are not expected to occur.[53]

A discrepancy remains in connection with the magnetization $\langle M \rangle$ as a function of H deduced from the magnitude of the field-induced conductance dip $\Delta G(0, H)$, shown in Fig. 25. The choice $\langle M \rangle = \tanh(\frac{1}{2}\beta\Delta)$, for $S = \frac{1}{2}$, saturates much too rapidly; the approximate form $\langle M \rangle = S(\Delta)$, from (2.38), which would correctly describe an inhomogeneous distribution of widths Γ, provides an improvement but also saturates too rapidly. While a rigorous generalization of the derivation of $\langle S_z \rangle$ to the case of large broadening $\Gamma \sim g\mu_B H$ is needed, this alone may not fully explain the behavior.

The possibility appears that the observed failure of $\langle M \rangle$ to saturate is characteristic of the Anderson model in the strong-coupling limit, when conduction electrons are rapidly hopping on and off the local site. Alternatively, one can say that conduction-electron wave functions are strongly admixed into the localized state. A plausible consequence might be modification of the magnetization from a Brillouin function to a behavior closer to the conduction-electron magnetization $\langle M \rangle = \tilde{\chi}_P H$, which does not saturate. The conjecture that a nonsaturating Pauli component may be mixed into the magnetization for large V_{kd} is given some support by recent work on the Anderson model[20] not restricted to $\Gamma_A/U \ll 1$. A change in the temperature dependence of the susceptibility of the local moment from the Curie law $\chi \propto 1/T$ at $\Gamma_A/U \to 0$ to a temperature-independent Pauli susceptibility at $\Gamma_A/U \gg 1$ is predicted. Although the functional dependence of the magnetization on H is not reported, such a change in the temperature dependence might well be accompanied by the corresponding change in magnetic field dependence. Comparison with the new theory[20] on this point (as well as on the g values and magnetic-field-induced broadening) would be of considerable interest.

Finally, the comparison shown in Fig. 8 between the CDMT theory and the conductance background is regarded as satisfactory, although it is not as close as the comparison reported[17] for Pb|Ge: (7.5×10^{18} cm^{-3} Sb) junctions. The analysis in Sec. II C indicates that fluctuations in barrier thickness, arising from statistical fluctuations in the number of ions, are important in the present case, but almost negligible in the case of the Pb|Ge:Sb junctions.[17] One should realize that the importance of fluctuation effects is a general feature of thin tunneling barriers,[54,55] which is thought to account in various metal-insulator-metal and p–n tunnel junctions for conductances consistently exceeding the theoretical values.[55] Indeed, the Schottky-barrier junctions appear unique in that the effect of fluctuations can be readily estimated and either neglected, as we have justified (above) for the Pb|Ge junctions,[17] or corrected for, as in the

present case. Further work is required, however, in refining the analysis of Sec. II C and in extending it to study the possible influence of fluctuation effects on the bias dependence of the conductance $G(V)$.

VI. CONCLUSION

Taken as a whole, the experimental procedures and measurements, the CDMT[16] and Kondo[1]–Appelbaum[6] theories, and the Anderson[7,33] and localized donor[11] models provide a remarkably comprehensive, usually quantitative understanding of elastic, spin-flip, and Kondo tunneling in the vacuum-cleaved Schottky-barrier junctions which have been studied. A reasonably complete understanding of the As and P local magnetic moments and their s–d exchange coupling, Eq. (1.1), has been achieved. Most of the specific conclusions have been included in the abstract and Table I.

Extension of these measurements to lower temperatures to verify the revised estimates $T_K = 0.7\ ^\circ\mathrm{K}$ for Si : P and $T_K = 0.3\ ^\circ\mathrm{K}$ for Si : As is feasible and might complete a self-consistent specification of all parameters of the s–d exchange-coupled moment. More importantly, this should permit a spectroscopic study of the "condensed state" and a check on the various theories.[2-5] To make such an interpretation unequivocal, it would be necessary to rule out effects from interaction between moments and to determine that the intrinsic level widths of the final states do not exceed $k_B T_K$. While this could be challenging, there is to our knowledge no other tunneling system in which as many of the relevant parameters are specified.

Another topic on which further work is indicated, in our opinion, is the magnetization $\langle M \rangle$ of a localized moment as a function of H, in the presence of large broadening $\Gamma \sim g\mu_B H$ and in connection with the Anderson model in the case $\Gamma_A/U \sim 1$.

It appears from the present work and that reported in Refs. 16, 17, and 50 that in the vacuum-cleaved metal-semiconductor tunnel junctions to which the model of Conley, Duke, Mahan, and Tiemann[16] applies, at least semiquantitative agreement is observed between the theory, using independently measured barrier parameters, and the tunneling conductance. This is an advance that should contribute both to the design of new experiments and to confident analysis of observed spectra.

In addition, in the present experiment we have demonstrated that the final states in the electrode, whose properties are revealed in the background conductance, are representative of the bulk of the electrode[50,51,56] rather than of a region close to the barrier. As well as providing detailed information regarding the interface region, such as that obtained in the present study of exchange-coupled magnetic moments, we anticipate that metal–degenerate-semiconductor tunneling experiments will provide additional spectroscopic information concerning interactions in the bulk electrode.

Note added in proof. Measurements at zero field have recently been extended to $0.13\ ^\circ\mathrm{K}$ and do confirm the predicted difference between Si : As and Si : P at very low temperature. The new data, consistent with that in Fig. 11, show a reduction of $G^{(3)}(0)$ from the $\log T$ dependence below $0.4\ ^\circ\mathrm{K}$ for Si : As and below $1.0\ ^\circ\mathrm{K}$ for Si : P. In the latter case $G^{(3)}(0)$ is nearly constant below $0.2\ ^\circ\mathrm{K}$; hence we believe that the voltage dependence for Si : P at $0.13\ ^\circ\mathrm{K}$ represents the Kondo scattering spectrum well below T_K. A report of this work will be submitted shortly.

ACKNOWLEDGMENTS

It is a pleasure to acknowledge the advice and assistance of L. G. Rubin in performing experiments at the Francis Bitter National Magnet Laboratory. We also thank Dr. Paul Nielsen for kindly measuring our Si : As junction below $1\ ^\circ\mathrm{K}$. We have had many useful discussions with Professor K. H. Bennemann, and wish to thank Dr. R. P. Khosla and J. R. Fischer for making transport measurements.

---

*Visiting Scientist, Francis Bitter National Magnet Laboratory.

[1] J. Kondo, Progr. Theoret. Phys. (Kyoto) 32, 37 (1964).

[2] A. A. Abrikosov, Zh. Eksperim. i Teor. Fiz. 48, 990 (1965) [Soviet Phys. JETP 21, 660 (1965)].

[3] H. Suhl, Phys. Rev. 138, A515 (1965).

[4] Y. Nagaoka, Phys. Rev. 138, A1112 (1965).

[5] D. R. Hamann, Phys. Rev. 158, 570 (1967); 186, 549 (1969).

[6] J. A. Appelbaum, Phys. Rev. Letters 17, 91 (1966); Phys. Rev. 154, 633 (1967).

[7] P. W. Anderson, Phys. Rev.. Letters 17, 95 (1966).

[8] K. Yosida, Phys. Rev. 106, 893 (1957).

[9] M. B. Walker, Phys. Rev. 176, 432 (1968). Note that the width Γ is not to be confused with the broadening Γ_A in the Anderson model.

[10] Y. Wang and D. J. Scalapino, Phys. Rev. 175, 734 (1968).

[11] E. L. Wolf and D. L. Losee, Solid State Commun. 7, 665 (1969); Phys. Letters 29A, 335 (1969).

[12] D. L. Losee and E. L. Wolf, Phys. Rev. Letters 23, 1457 (1969).

[13] L. Y. L. Shen and J. M. Rowell, Phys. Rev. 165, 566 (1968).

[14] C. B. Duke, in *Solid State Physics*, edited by F. Seitz, D. Turnbull, and H. Ehrenreich (Academic, New York, 1969), Suppl. Vol. 10, p. 161.

[15] E. L. Wolf and W. D. Compton, Rev. Sci. Instr. 40, 1497 (1969).

[16] J. W. Conley, C. B. Duke, G. D. Mahan, and J. J. Tiemann, Phys. Rev. 150, 466 (1966).

[17]F. Steinrisser, L. C. Davis, and C. B. Duke, Phys. Rev. 176, 912 (1968).

[18]J. Kondo, Progr. Theoret. Phys. (Kyoto) 28, 846 (1962).

[19]J. R. Schrieffer and P. A. Wolff, Phys. Rev. 149, 491 (1966).

[20]S. Q. Wang, W. E. Evenson, and J. R. Schrieffer, Phys. Rev. Letters 23, 92 (1969).

[21]H. Suhl, Phys. Rev. Letters 20, 656 (1968).

[22]D. Gainon and A. J. Heeger, Phys. Rev. Letters 22, 1420 (1969); K. H. Bennemann (private communication).

[23]David L. Cowan, Phys. Rev. Letters 18, 770 (1967).

[24]C. A. Mead and W. Spitzer, Phys. Rev. 134, A713 (1964).

[25]J. Bardeen, Phys. Rev. 71, 717 (1947); V. Heine, *ibid.* 138, A1689 (1965).

[26]J. W. Conley and G. D. Mahan, Phys. Rev. 161, 681 (1966).

[27]R. Stratton and F. Padovani, Phys. Rev. 175, 1072 (1968).

[28]G. H. Parker and C. A. Mead, Phys. Rev. 184, 780 (1969).

[29]A. Honig, Phys. Rev. Letters 17, 186 (1966).

[30]A. Honig and R. Maxwell, in *Proceedings of the Ninth International Conference on the Physics of Semiconductors*, edited by S. M. Ryvkin (Nauka Publishing House, Leningrad, 1968).

[31]G. Feher, Phys. Rev. 114, 1219 (1959); G. Feher and E. A. Gere, *ibid.* 114, 1245 (1959).

[32]M. N. Alexander and D. F. Holcomb, Rev. Mod. Phys. 40, 815 (1968).

[33]P. W. Anderson, Phys. Rev. 124, 41 (1961).

[34]J. Hubbard, Proc. Roy. Soc. (London) A281, 401 (1964).

[35]D. Pines, J. Bardeen, and C. P. Slichter, Phys. Rev. 106, 489 (1957).

[36]C. Yamanouchi, K. Mizuguchi, and W. Sasaki, J. Phys. Soc. Japan 22, 859 (1967).

[37]R. P. Khosla (private communication).

[38]G. W. Gobeli and F. G. Allen, J. Phys. Chem. Solids 14, 23 (1960).

[39]J. G. Adler and J. E. Jackson, Rev. Sci. Instr. 37, 1049 (1966).

[40]P. Nielson (private communication). We are indebted to Dr. Nielsen for studying our sample below 1 °K.

[41]R. J. Archer and M. M. Atalla, Ann. Acad. Sci. (N. Y.) 101, 697 (1963).

[42]L. Kleinman, Phys. Rev. 140, A637 (1965).

[43]This is in accord with estimates of the interaction strength based on our previous estimate of ~ 150 Å as the spacing between moments. Note that the Anderson width Γ_A does not appear as a zero-field Zeeman-level width since it can be transformed out of the spin problem, as Schrieffer and Wolff have shown. Hence Γ_A is not implied to be smaller than 3×10^{-5} eV, and there is no conflict with the estimate $\Gamma_A \approx 0.6$ meV, which follows from Eq. (2.53) with $U \approx 2E_0 \approx 4$ meV.

[44]Much larger values of E_0 in metal-insulator-metal junctions have been reported by P. Nielsen, Solid State Commun. 7, 1429 (1969); Phys. Rev. (to be published).

[45]A general discussion is given by Conyers Herring, in *Magnetism*, edited by G. T. Rado and H. Suhl (Academic, New York, 1966), Vol. IV.

[46]K. Fischer, Phys. Rev. 158, 613 (1967).

[47]J. Kondo, Phys. Rev. 169, 437 (1968).

[48]J. A. Blackman and R. J. Elliott, J. Phys. C 2, 2099 (1969).

[49]It is possible to obtain an estimate of g_0 from high-field measurements alone by setting the observed broadening $\Gamma_{obs} = \frac{1}{4}\pi (g_0-g)^2 g\mu_B H$, and using measured values of g and $g\mu_B H$. This procedure, carried out for Si : As, gives $g_0 = 2.1$ We prefer to take $g_0 = 2.0$, based on the local moment model, and to use the comparison of experimental and theoretical values of Γ as a test of consistency in the analysis.

[50]D. L. Losee and E. L. Wolf, Phys. Rev. 187, 925 (1969).

[51]D. C. Tsui, Phys. Rev. Letters 21, 994 (1968).

[52]A. G. Chynoweth, R. A. Logan, and D. E. Thomas, Phys. Rev. 125, 877 (1962); see also Ref. 13.

[53]This accounts for the absence of the conductance peak in vacuum-cleaved Schottky-barrier junctions on Ge: (7.5×10^{18} cm^{-3} Sb) reported in Ref. 17. The Mott concentration given in Ref. 32 for Ge : Sb is 0.95×10^{17} cm^{-3}. The donor concentration in the junctions studied is thus $\approx 80N_c$, as compared to $\approx 4N_c$ in the present case.

[54]I. Giaever, in *Tunneling Phenomena in Solids*, edited by E. Burstein and S. Lundqvist (Plenum, New York, 1969), p. 25.

[55]C. B. Duke, Ref. 14, p. 221.

[56]E. L. Wolf, Phys. Rev. Letters 20, 204 (1968); L. C. Davis and C. B. Duke, Solid State Commun. 6, 193 (1969). See also D. E. Cullen, E. L. Wolf, and W. D. Compton, Phys. Rev. B 2, 3151 (1970).